POLITECNICO DI MILANO

Dipartimento di Chimica, Materiali ed Ingegneria Chimica "G. Natta"

Tesi di Laurea in Ingegneria Chimica

Relatore: Prof. Maurizio MASI

Autore: Edoardo RAFFA

Matricola: 735971

Index

Introduction

In the recent years, many studies (IEA International Energy Agency, 2007; Smalley R. E., 2005) have shown that the extensive use of the solar energy is not certainly limited by territory extension limits but rather from the availability of photovoltaic devices able to realize high conversion with costs comparable with those of the today main resources. In fact, the raw material and the process costs are determinant about the success of the adopted conversion technology. Because of the synergies with the microelectronic industry, the largely adopted material in photovoltaic cells production is silicon, which can be produced at high purity and at reasonable prices and is the semiconductor material most abundant in nature. The crystalline silicon cells (single- crystal, massive or ribbon poly-crystal) today covers about 93% of the global photovoltaic market, with the prevailing share (56%) for polycrystalline ones (Rogol M., 2004). Among the cell cost reduction frame, it is clear that the main costs are substantially linked to the amount of material needed for the cell manufacture and, indeed, increasingly high attention is nowadays focused on thin film technology, where a thin film of semiconductor material is deposited onto a low cost substrate like glass. Nevertheless, the transition towards thin film technology by itself cannot permit the increase in process productivity as great as that necessary to provide enough economic benefit for widespread commercialization of low cost thin film solar cells. Therefore, further cost reduction plans must be developed. In particular, potential solutions should be focused to the development of reduction pathways addressing the process cost than the material one. In fact, in the deposition process for amorphous or nano-crystalline silicon thin films, today realized with the low pressure plasma enhanced chemical vapor deposition technique (PECVD), the main cost is represented by sustaining the vacuum and by generating the electric discharge necessary to sustain energetically the deposition system. Therefore, energy saving production processes appears as promising choices and seem to prospect the development of technologies not involving the use of vacuum conditions and electrical input heating. These last two necessary process features can be thus directly translated in the term atmospheric pressure (AP) conditions and auto-thermal management of the deposition reactor. Furthermore, process “flexibility” over a relatively wide range of operating conditions, in terms of process productivity (*e.g.*, growth rate, precursor conversion) and material quality (*i.e.*, surface proprieties), is an important feature for any innovative manufacturing process. Last but not least, the opportunity to run the process in a continuous manner can represent a huge advantages in terms of economical benefit (Masi M. et al., 1997; Nieto J.P. et al., 2005; Chiu W.K.S. et al., 2000).

Recently, among the wide variety of deposition techniques, flame assisted chemical vapor deposition (FACVD) processes have been proposed, in combination with the hydrogen-halogen flame, for the growth of bulk semiconductors by members of our research team[1]. Since from the early research works, the attention has been focused mainly on silicon dioxide film manufacturing and high growth rate diamond synthesis (Tzeng Y. et al., 1991 and 1988; Yarbrough W.A. et al., 1989 in references therein). In particular, for the process operating under AP and high temperature (HT) conditions, accordingly to the well established existing theory of CVD, the main physical mechanism governing the deposited material growth is the mass transfer. It is also well known (Masi M. et al., 2003) that the thermo-fluid fields developed in front of the susceptor strongly influence the deposition rate as well as the microscopic crystal surface proprieties, as multi-scale approaches well highlighted (Masi M., 2001 and 2009; Barbato A. et al., 2007). In fact, it is well known that many surface proprieties of the deposited material depend on the dimensionless ratio between the surface diffusion rate and the crystal growth one (Bloem J., 1980; Gilmer G. H. et al., 1986; Venables J. A. et al., 1984; Madhukar A. et al., 1988). The fundamental experimental work of Bloem et al. (Bloem J., 1980) have firstly demonstrate how growth rate controls the morphology of silicon films. Generally, increasing the rate of arrival causes a decrease in the degree of crystalline order for the polycrystalline-to-amorphous transition in the 550–650°C range and the single crystal-to-polycrystalline transition in the 1000–1400°C.

[1] Patent: ITMI20051308,WO2007006525,EP1907609.

Moreover, the lower the temperature of deposition, the lower the growth rate must be to accommodate a given level of crystal perfection. It is this concept that controls the growth rate/temperature conditions used in commercial silicon deposition technology, where indeed amorphous and epitaxial crystals can be produced under low temperature (surface diffusion limited process) or HT (film diffusion limited process) conditions, respectively.

Nevertheless, even if the manufacturing tolerances for photovoltaic thin silicon film production are generally not as restrictive as those for microelectronics, variations in film properties can lower the cell efficiency and, thus, a proper understanding of the process variables governing crystal growth is clearly crucial, especially to optimize the reactor performance at the pilot plant as well as at the industrial scale. Moreover, as in the industrial FACVD reactors used for diamond synthesis, HT gradients across the flame sheet and near the susceptor and reactor walls produce density variations leading to buoyancy driven secondary recirculating paths superimposed on the main flow. The resulting convective mixing adversely effects the film thickness and the composition uniformity.

The aim of this work is to develop, through a systematic computational strategy, a novel predictive multi-hierarchical model able to optimize the performance (in term of process productivity and economic benefit) of the prototype FACVD reactor[1], here proposed as novel reactor for thin polycrystalline silicon films production via the two main industrially common rote: silane (SiH_4) and trichlorosilane ($SiHCl_3$) precursors. Its design features permit to set, at its inlet, different burner geometries (single, porous or multiple nozzles (MN) burner) in order to exploit the advantages of the two classical stagnation flow and Bunsen stretched flames. The former yields type of stagnation flow, which, aside from unavoidable edge effects, is inherently scalable to large deposition areas, as many authors suggested (Goodwin D.G. et al., 1993; Glumac N.G. et al., 1993) and Murayama et al. (Murayama M. et al., 1992) convincingly demonstrate for diamond synthesis.

Although some researcher groups recently suggest to lower the pressure in order to flatten and stabilize the flame front (Goodwin D.G., 1993), the opportunity to investigate the advantages of multiple Bunsen flames burner at AP conditions, in order to achieve enhanced process performance, good material quality as well as economical benefit, operating at HT in auto-thermal manner, are particularly addressed here. In fact, Tzeng et al. (Tzeng Y. et al., 1991) experimentally demonstrated that large area (up to 20 mm in diameter) diamond films can be deposited at low expense in uniformity of the quality of the deposited materials if the gas flow through each nozzle is controlled separately.

Contrarily to the conventional non-flame CVD, in FACVD many different physical mechanisms can govern fluid, momentum, energy and mass transfer depending on the reactor geometry and process operating conditions. In fact, because of the generally HT gradients developed between the unburnt and burnt mixtures and near the susceptor or reactor walls, thermo-fluid field have a dramatic effect on the value of the overall growth rate in terms of productivity and of the quality of the deposited material. Moreover, entrainment flow and rolls are really present, especially for Bunsen flame assisted deposition methods. In fact, the diamond films obtained by this technique are not uniform, and the deposition areas are rather small (Hirose Y. et al., 1988). The small area is a consequence of conical flames, in which distributions of temperature and radicals' concentrations are complicated and nonuniform against the substrate. Moreover, expect for marginal issues (Okkerse M. et al., 1991), the experimental data well agree with the model-based results, as the computational and experimental works of Klejin and coworkers (Okkerse M. et al., 2000) well highlighted for single nozzle, impinging Bunsen flame, diamond synthesis, reactor. However, fortunately, it has been demonstrated that a uniform deposition of diamond can be attained by means of a flat flame stabilized near the stagnation point of a substrate (Murayama M. et al., 1992). Under the investigated experimental conditions, the premixed inner flame lifted-off the burner rim and a flat flame was obtained in front of the substrate, due to the use of mantle flow and converging nozzle. The theoretical works developed by some research groups (Glumac N. G. et al., 1992 and 1993; Kim J. S. et al., 1992, 1998; Meeks E. et al., 1993) for the optimization of this stagnation flow reactors are similar to those used for stagnation flow flame, but clearly additional equations

(representing the mass flux continuity at wafer surface and the law of mass conservation for surface species) were introduced because, for the operating condition generally achieved (*i.e.*, low pressure and HT), surface kinetics controls the deposition rate. Nevertheless, as the comparison between modeling results and experimental data well evidences, when the flow velocity is too fast, the stretch rate of the flow is so large that the inner flame is blown off at the stagnation point. In fact, proper control and flame stability are two main still unsolved critical disadvantages of stagnation flow technique. Moreover, flame stability are ensured only for limited range of flow rate and "standoff" distance – the height between the injector nozzle exit and the target susceptor. Least but not least, the scale-up to large area products can be achieved only by lowering the pressure and, hence, with increasing the process cost.

On the modeling side, the combustion CVD combines the difficulties encountered in laminar flame simulations with those of classical thermal CVD modeling. For conventional (batch manufacturing) thermal CVD processes, where gas-phase and surface reactions do not release significant amounts of heat, it has proved possible to design a reactor with the aid of CFD. In fact, model based approaches surely represents a valid tool in order to control the final product quality as well as in narrowing the range of conditions which must be investigated experimentally. Moreover, a proper computational reactor design optimization usually permits to minimize (even for edge zones) the effect of temperature and velocity gradients on film thickness (*i.e.*, growth rate) distributions along both radial and axial coordinates (Masi M. et al., 2003). Least but not least, they can be used for reliable scale-up strategies , once the process feasibility had been experimental demonstrated.

In the field of laminar flame simulations, two approaches can be distinguished: study of detailed combustion chemistry with the aid of zero- or one-dimensional hydrodynamic models (*e.g.*, Rota R. et al., 1995) and the more rigorous investigations with the aid of two-dimensional CFD simulations, using lumped chemistry (*e.g.*, Bennett B.A.V. et al., 1998; de Lange H.C., 1994). Excellent works (Smooke D.M., 1982; Giovangigli V., 1987; Heimerl et al., 1890), reviews (Kailasantath et al., 1982) and books (Warnatz et al., 1982; Smooke D.M., 1991) summarized the features of the most common steady-state and transient one-dimensional laminar flame models together with detailed discussion about some industrial applications. Moreover, Law et al. (Law C.K. et al., 2000) reviewed and presented in a tutorial manner the modeling aid in the understanding of the propriety of laminar premixed flames under the influence of stretch, as manifested by aerodynamic straining, flame curvature, and flame/flow unsteadiness.

The geometry of premixed stagnation flow laminar flames is of fundamental and practical interest in the study of the combustion of premixed gaseous flows, because it is one of the few chemically-reacting systems that admit, under certain approximations, a similarity transformation, which permits to reduce the complete three-dimensional set of governing equations (Kou K.K., 1986) to one-dimensional problem. Such aid greatly facilitates the mathematical treatments and the physical interpretation of the main factors influencing the flame proprieties, as the valuable analytical solutions (Sivashinsky G.I., 1976; Buckmaster J., 1982; Cremers M.F.G. et al., 2007 and reference therein) and robust numerical codes (PREMIX; Smooke M.D., 1982; Smooke M.D et al., 1983; Sato J. et al., 1983; Giovangigli V. , 1986; Smith H.W. et al.; 1971; Somers L.M.T., 1994; Darabiha N. et al., 1985; Sermange M., 1985; Dixon-Lewis, 1967) available in literature clearly demonstrated. The more recently developed numerical codes have the ability to calculate the velocity, temperature and concentration profiles as well as adiabatic flame speeds (PREMIX; Smooke M.D., 1982; Smooke M.D et al., 1983; Grcar et al., 1985 and 1988; Kee R.J. et al., 1980; Somers L.M.T., 1994) – and, thus, are generally referred as direct numerical simulations (DNS) –, while the so-called *decoupled* approaches (Olsson J.0. et al., 1985 and 1986) permit to analyze a number of flame proprieties once a known temperature or concentration profiles are superimposed on the complete set of modeling equations. The latter – also called direct *experimental* approach (Dixon-Lewis G., 1968) because the fixed profiles usually are been derived from experimental data – is commonly use to provide starting values for the time-dependent former, and also in order to low the computational effort and numerical instability (especially for lifted flames). Moreover, the excellent

agreement with a wide variety of experimental data sets of different authors (Dixon-Lewis G., 1979 and 1968) has historically contribute to place them as “standard” simulation tool to study the structure, extinction and stability for stagnation-point laminar flames (Mukunda, 1968; Dixon-Lewis G., 1996; Law C.K. 1998, Kee R.J. et al., 1998). Nevertheless, it has been experimentally and computationally demonstrated (Cuenot et al., 2008) that the reliability of these two approaches in predicting the flame proprieties depends strongly on the fluid dynamics and heat transfer mechanisms developed in the system. In fact, in spite of its importance, a critical review (Andrews G. E., 1972) of past experimental measurements of laminar flame speed has surprisingly shown a very wide scatter that can hardly be attributed to experimental uncertainties related to instrumentation and/or procedures. It has been subsequently realized, however, that the source of this scatter is the fact that the ideal one-dimensional flame model can not be reproduced in the laboratory, as premixed flames must be stabilized either through heat loss, curvature, and/or aerodynamic straining (Law C.K., 1988). Thus, in many existing measurements the effects of these not negligible external mechanisms have not been systematically taken into account. Nevertheless, as example, the inlet flow rate (even if in the laminar range) can strongly affect the flamelet structure, which can translate from (perfectly or partially) premixed to diffusion models (Cuenot et al., 2008). In fact, the fluid paths developed in the preflame zone can lift-off the flame front and, as the flame is bring close to the cold substrate, blow-off or extinction can occur. Moreover, Hsieh W.D. et al. (Hsieh W.D. et al., 2005) experimentally demonstrated that the combined effects of the curvature stretch and the aerodynamic straining dramatically affect the flame shapes even at fixed flow conditions and system geometry, which exhibit double-solution characteristics in a certain range of oxy-to-fuel ratio. Nevertheless, only a very limited amount of research has been devoted to studying the behavior of a conical Bunsen flame established in a stagnation flow (Hsieh W.D. et al., 2005).

Surely higher order approaches (especially the two-dimensional one) permits to removed the idealizations necessarily introduced for 0-D and 1-D models and, therefore, edges and buoyancy effects (*e.g.*, preferential fluid paths and rolls) as well as lift-off really present in many configurations, under certain operating conditions, can be properly simulated and understood.

For Bunsen flames, analytical (Cremers M.F.G. et al., 2004, 2006(3), 2007(2), 2008(2) and 2010) and numerical models are available in literature (Bennett et al., 1998 and 1999; Valdati, 1997; Takagi T. et al., 1996; Frouzakis C. E. et al., 1998; Schönfeld T. et al., 1998 and 1999). However, as the recent analytical treatments of Cremers and coworkers (Cremers M.F.G. et al., 2010) evidence, analytical model are mainly focused on the prediction of the postflame velocity fields and heat transfer rate for Bunsen flame impinging onto a target surface. Moreover, the laminar flame speed is an model input parameter. Nevertheless, the lack of reliable experimental data over a wide range of operating conditions – for the here considered hydrogen-chlorine flame – permits to use this approach only for *a posteriori* investigation of the validity of the ideal flow hypothesis. However, as the same authors suggested (Cremers M.F.G. et al., 2006), the analytical solutions of the stagnation point heat transfer flux surely represent a valid aid in the understanding of the role played by susceptor temperature on the stagnation point heat transfer rate. Moreover, as for the stagnation flow models, ideal one-dimensional approaches neglect the effects of wall confinement, buoyancy and flame stabilization mechanisms. Accordingly, in the last decades, the attention is focused on the development of two-dimensional finite element methods. Careful consideration must also be devoted to the grid-refinement strategies mainly because the model robustness of the finite element methods strongly affects the model validation filed, especially for complex geometry or confined systems. In fact, in the past decades, advance grid-refinement strategies have been proposed by many authors (especially for transient computational study). However, the enhanced performances of some commercially available finite element codes (COMSOL, PHOENICS) offers the opportunity to impose the required grid-refinements at negligible expense of the computational effort. In particular, as the work of de Lange and coworkers (de Lange, 1992; de Lange et al., 1994) – focused on the development of locally refined

non-staggered grid – clearly demonstrated, if grid points are added to a coarse grid in areas where a given property has large gradients the solver algorithm reached the solution rapidly. Moreover, as the same authors noted (de Lange et al., 1994), uniform grid have several advantages over truly non-uniform grid. In fact, the former can be represented by simple data structures, simple accurate discretization stencils and fast solution techniques are available for solving the system of equations resulting from it. In more recent works (Giovangigli and coworkers, 2007), it has been demonstrated that an improved finite element method – based on the extension to chemically reacting flows of the streamline diffusion method – permits to study the impact of inflow velocity profiles on the structure of several hydrogen–air Bunsen flames. In particular, their robust solution algorithm includes least-squares stabilization of the pressure gradient and shock capturing term designed to control species mass fraction undershoots near flame fronts.

Accordingly, a modular and hierarchical structure should be adopted in order to highlight the individual contribution of each physical mechanism governing a particular process. Accordingly, the here developed model framework offers the opportunity to describe the reactor performance through zero-order (0-D) or first-order (1-D) or second-order (2-D) models. These overall models are also composed by a number of (analytical of numerical) sub-models, each of them addressing a set of process occurring in the reactor (fluid flow, heat and mass transfer or chemical reactions), which are solved through a decoupled two steps procedure. The modularity the here used computational simulation strategy permit to implement analytical or simplified sub-models into higher-order approaches.

The simplest adopted 0-D model consist of a heterogeneous perfectly mixed (or continuous stirred) ideal reactor (CSTR) model; a simplified approach followed by some authors for study the main important aspects of plasma torch (Dandy et al., 2010; Meeks E. et al., 1996) and diamond synthesis (Okkerse M. et al., 2000) reactors. The effects of flame is taken into account only by the introduction of a combustion chemical kinetic mechanism in the gas phase reactions data sets (neglecting the thermo-fluid dynamic structure of the flowing gas mixture) in order to estimate the maximum gas phase temperature, for adiabatic or isothermal systems. An extended version of the in-house numerical CSTR.rad Fortran code are developed in order to take into account the mass transfer resistances. The classical non-Soret Fickian diffusion models is adopted as multicomponent transport algorithm. The main disadvantages of this 0-D approach is that it cannot properly take into account the effects of reactor geometry and flame structure. Nevertheless, it can provide average values of film thickness distribution, bulk or surface precursors compositions and maximum flame temperature. In fact, its main aid is in narrowing the range of conditions for the forthcoming experimental investigations and, due to its low computational cost, it can also permit to decoupled reactor and flame calculations, as the work of Goodwin et al. (Goodwin et al., 1998) – where the reactor inlet conditions implemented for 1-D model reflects the post-flame adiabatic equilibrium composition calculated through a CSTR model – suggests. Finally, in contrast to the detailed reactor models, this simplified approach can be executed in near real-time on a computer of model size, and can therefore be readily incorporated into process control models or global dynamics loop simulations.

A better reactor optimization can be achieved through 1-D models, where the variations of reacting mixture proprieties along the centerline of the axisymmetric systems are investigated. In particular, in order to simulate heat transfer (from laminar, perfectly premixed, flame) and growth rate near the stagnation point, different already published analytical model (Cremers M.F.G. et al., 2007) and commercial codes (PREMIX) as well as here developed decoupled approaches are used. In fact, to study the chemical phenomena pertinent to stagnation-point planar, strained, premixed flames, the “one dimensional analysis” can provide a valuable development, validation, and optimization test bed for transport and kinetics models, even though the experimental flame may be geometrically complex (Miller et al. 1990). Moreover, the model structure permits to implement analytical expressions for “ideal” flow paths, temperature distributions and reduced order kinetic mechanisms in order to shoot down the computational cost at negligible expense on the model sensitivity. Many authors (Pohlhausen et al.,

1921; Fairwather et al., 1983; Cremers M.F.G. et al., 2004, 2006(3), 2007(2), 2008(2) and 2010) indeed derived one-dimensional analytical expressions for flame jet impingement heat transfer rate near stagnation point by solving the continuity and momentum equations. In fact, under reliable approximations, the energy balance equation (*i.e.*, the temperature distribution) can also be decoupled from the momentum equation (*i.e.*, the velocity field). Such an approach highlights the opportunity to analytically treat the thermo-fluid problems for the two regions separated by the flame front: the potential core (preflame) zone and the stagnation flow or jet-flow (postflame) regions. In particular, the local thermochemical equilibrium approach permits to "turn-off" the gas phase kinetics and calculate the equilibrium mixture compositions along the post-flame region, because the primary (70-90%) heat loss mechanism are axial downstream convection towards the relatively cool substrate when flame temperatures is lower than approximately 1700 K (Baukal C.E. et al., 1996; Jackson E.G. et al., 1956; Béer J.M. et al., 1968; Milson A., 1973). These analytical models are here implemented in a two steps procedure, similar to that developed by other authors (Okkerse M., 2000; Pons M. et al., 1989), in order to lower the numerical computational effort: the momentum, energy and mass balances for each species involved in the flame chemistry are first solved and the calculated velocity, pressure and temperature fields become inputs to precursor species conservation equations, while the consumption of the reacting gas stream (*i.e.*, the deposition rate) is represented by a boundary condition on the reacting areas. However, such an approach is valid if the concentration field of the precursors species slightly affects the thermo-fluid aspects. This generally happens for highly diluted regime (*i.e.* inlet precursor mass fraction less than 5% vol). Moreover, the concentration profiles in the gas phase calculated by this *decoupled* approach are compared with those calculated under the local equilibrium approximation (*i.e.*, mixture at thermodynamic equilibrium), which are expected to adequately represent the real silicon gas precursors composition for AP and HT conditions, as the high gas phase and surface Damköhler numbers (typically around about 10^2) suggests.

Finally, 1-D simulations are performed by direct numerical simulation (DNS) of all involved processes (Navier-Stokes weakly-compressible flow, energy and mass transfer as well as combustion and deposition chemical reactions) by means of the commercial available finite element Chemkin code (Chemkin-III).

Numerical 2-D models permit to gain insight on the role played by the different mechanisms governing the process and, therefore, can aid in the optimization of the reactor performance, mainly in term of uniformity along the radial coordinate of the wafer. More complex reactor configurations (particularly MN burner) can also be simulated and their advantages can be well understood and quantified. As mentioned for the 1-D models, lumped chemical kinetic schemes and decoupled approach permit to reduce the computational effort, while parametric sensitivity analysis can be used to aid model validating. Nevertheless, because of the confined configurations (*e.g.*, short nozzle-susceptor separation distance), although the general validity of the simplified approach introduced above still hold within the stagnation zone(s), some phenomena not taken into account in the 1-D model are particularly addressed in this work. In fact, the preferential fluid paths, the onset of HT and high concentration gradients due to the spontaneous entrainment or recirculation of outside cold fluid streams can strongly affect the flame structure and properties, the gas temperature distribution (*i.e.*, the heat transfer rate or the local Nusselt number distribution) as well as the precursor species distributions (*i.e.*, the local Sherwood number distribution). In particular, for MN burner, the shroud flow(s) of hydrogen from the nozzle(s) surrounding the central reactant gas jet, used to prevent formation of a conical flame of the reactant gases stabilized on the nozzle rim (together with short nozzle-target separation distance) can produce undesired preferential fluid paths, rolls and stagnation regions. Moreover, entrainment flow strongly affect the boundary layer thickness distribution along the susceptor as well as the burnt mixture compositions near the edge of the deposition substrate. Finally, since it was experimentally as well as computationally demonstrated that the inverted (upside-down) orientation has clearly advantages in terms of providing good uniformity and ideal flow fields, the 2-D reactor orientation is not addressed here.

As in classical non-combustion environments, the development of three-dimensional models (which can dramatically increase the computational efforts) should be adopted only to verify solutions previously identified through simplified models addressing only partial aspects of the problem. In fact, the computations of Kleijn and coworkers (Santen H.V. et al., 2000) have clearly shown that 2-D axisymmetric flow is a good assumption except under conditions where strong natural convection exists.

Detailed multicomponent transport models usually include rigorous treatments of diffusional fluxes that are important in noncombustion CVD because their presence is required for the accurate calculation of the concentrations of important species and of important features. In addition, they necessarily include the dependence of the diffusion coefficient matrix and physico-chemical proprieties on temperature, pressure and composition, which also can be now considered a mature field, as the high number of transport libraries demonstrates. Moreover, although a wide variety of algorithms for multispecies transport fluxes are available in literature (Jones et al., 1981, Smooke and coworkers), its inclusion usually requires the modification of general-purpose CFD codes, which may not be trivial, especially if source codes are not available (Klejin C.R., 1991). The use of simplified flux expressions in place of the general Stefan-Maxwell formulation in reacting flow computations is discussed in detail for combustion (Jensen. K.F. et al., 1993 and 1991 and references therein) and for CVD systems (Coltrin M.E. et al., 1986; Kleijn C.R., 1989). Under conditions where the precursor is dilute in the carrier gas, such as is almost the case of any epitaxial deposition, the effective diffusion coefficient can be set equal to the binary diffusion coefficient or it can be estimated by the relation given by the Blanc's formula (Bird R.B. et al., 2001). The thermal diffusion factor can be estimated through relationships based on the kinetic theory of gases (Hirschfelder J.O. et al., 1967) and usually is then interpolated as a third order polynomial function of temperature and composition

In this work, the impact of detailed transport models on the process performance, in terms of deposition rate and surface species concentration, is particularly addressed. Three different multicomponent transport algorithms are considered: first, the classical Fickian diffusion model, second, the non-Soret full multicomponent model, and third, the more rigorous Stefan-Maxwell approach.

Furthermore, although the modularity of the simulation strategy offers the opportunity to run the process at AP and HT conditions (*i.e.*, under diffusion limited regime), where the role played by gas phase reactions (which usually is in pressure falloff regime) and heterogeneous surface reactions can be neglected, an novel analytical treatment of heterogeneous surface reactions involved in silicon deposition kinetic mechanisms via chlorosilane route is proposed. Such a recent advance permit to gain insight on the individuation of the main reaction paths and a better understanding of the role played by the individual adsorbed species (in terms of adsorbed species coverage fractions) on the overall growth rate. Moreover, it can be easily implemented into the above introduced reactor models as well as in many commercially available codes.

Furthermore, although, the multi-hierarchical approach highlights the advantages to use models of varying complexity, the real engineering target is to predict the system behaviour in the easiest possible way and indeed simple models should also use parameters with a physically sound meaning, which can be independently estimated each one from the others and, most importantly, whose values were not fitted onto a particular set of data. For the here considered case of study, the model reduction issues can be translated in the following question: is it possible to use the same reaction mechanisms and multicomponent transport algorithms in spatially inhomogeneous multidimensional simulations that have been developed under spatially homogeneous conditions? In this paper, conditions and methods were selected in order to investigate specifically the thermal and diffusion couplings in all systems in a wide range of operating conditions. The initial and boundary conditions were chosen in such a way that the concentrations in all systems with and without thermal and diffusion couplings be as close as possible to each other.

Nevertheless, this global mapping issue is notoriously difficult for realistic problems typically involving a high dimensional space of parameters (Turànyi T. et al., 2002). On the contrary, because generally each model presents a sensitivity to its required inputs, parametric sensitivity analysis is an valuable tool in interpreting the results of different order approaches (Turànyi T., 1997; Turànyi T. et al., 2002; Varma A. et al., 1999; Tomovicand R. et al., 1972; Frank P.M. 1978). Accordingly, this advance computational tool is used here in order to individuate the deposition-driven species depending on the set of model input parameters, as the principal component analysis of the concentration sensitivity matrix usually used for finding reduced kinetic mechanisms. In particular, our attention is focused to the effect of inlet flow rate and susceptor temperature change to deposition rate and to the surface compositions. What must be highlighted is that, the change in these two objective sensitivities are strictly related to the role played by Soret thermal-diffusion effects. Our brutal force method numerical code (based on the first-order sensitivity coefficients evaluated by finite differences in a manner similar to the computation of the Jacobian) is valid only for steady-state solution (*i.e.*, see a characteristic ratio between growth and residence time of about 10^{-5}) and are implemented for 0-D and 1-D models. Moreover its computational efficiency exploits the fact that the differential equations describing the sensitivity coefficients are linear, regardless of any non-linearities in the model problem itself. The Jacobian and its LU factorization are already available from the solution of the original system and, therefore, the full linear system for each column of the sensitivity matrix corresponding to the sensitivities of the solution vector to each of the input parameters are therefore readily solve.

The hierarchy and modularity of the adopted approach can permit also to study to many other systems differing in terms of chemical kinetic mechanisms offering the opportunity to predict expected forthcoming experimental data sets. Indeed, predictive simulations for silicon oxide and silicon carbide films production processes are part of an ongoing research effort.

Summarily, the predictive reactor design approach developed here permits to computationally investigate and optimize the here considered prototype FACVD reactor performance and gain insight to the different physical mechanisms governing the crystal growth of thin silicon films in FACVD reactors under quite different reactor geometry and operating conditions.

Mathematical modeling

As mentioned in the Introduction, modularity and hierarchy represent the main features of our modeling approach. For shake of clarity, the discuss of the aspects related to the deposition and combustion kinetics precedes the detailed description of the three (0-D, 1-D and 2-D) overall models developed. For shake of brevity, although many calculations have been performed through already published computational treatments or commercially available codes, their derivation can be found elsewhere and are not in depth a here.

0D model – ideal CSTR model

The ideal perfectly mixed reactor represent a quite simple model in order to simulate FACVD processes, as some authors suggested (Dandy S.D. et al., 1995; AURORA). Our numerical code is implemented in the Fortran 90 programming language, being linked to the Chemkin thermodynamics and Chemkin mass transport databases (available in the same environment). The here adopted complete set of conservative equations and boundary conditions imposed at susceptor-vapor interface (*i.e.*, mass flux continuity and isothermal or adiabatic susceptor surface) well agree with the general framework reported elsewhere (Masi M. et al., 2001). Nevertheless, since the fluid and susceptor temperatures are model input parameters this simplified approach don't permit to gain insight the thermo-fluid aspects of the systems and the role played by system geometry and configuration. In fact, they are lumped into the reactor residence time (τ_R), temperature dependence of diffusion coefficient matrix and dependence of system average Sherwood number on Reynolds.

Such an approach is rigorously valid under nearly-perfect mixing. In fact, in many FACVD systems (where heated walls, entrainment flow, flame blow off or flame extinction have a dramatic impact on the fluid pattern developed in the reactor chamber), only a direct comparison of 2-D model simulations or reliable experimental data set, permits to validate this idealizations, which therefore cannot be confirmed only on the basis of the obtained 0-D model results.

1-D model – plug flow and ideal axisymmetric "flow" models

The simplest 1-D model decouples the fluid flow, energy and mass transfer as well as chemical kinetics.

Of particular interest is the implementation of analytical sub-models for the thermo-fluid aspects of the problem. Analytical treatments of flow filed for laminar stagnation flow and jet-flow configurations have been derived by Schlicting (Schlicting H., 1968 and references therein). For laminar premixed flame impingement problems (both stagnation flow flame and Bunsen flame), by using the reacting thermal conductivity concept[2] of Butler and Brokaw (Butler J.N. et al., 1957 and 1960) various authors (Pohlhausen et al., 1952; Fairwather et al., 1983; Cremers M.F.G. et al., 2004, 2006(3), 2007(2), 2008(2) and 2010) derived analytical expressions for the temperature distribution and stagnation point heat transfer rate for both adiabatic and isothermal boundary conditions. Moreover, these analytical investigations can elucidate the general trends in system behavior and parametric dependencies, and therefore can also be used as input or initial guess values for numerical simulations. In fact, as previously noted, detailed chemical kinetic schemes coupled to analytical or simplified thermo-fluid treatments may be computationally more desirable than DNS, especially for stiff problems. Accordingly, in order to lower the computational cost, a two-step solution procedure is developed (Okkerse M. et al., 2000; Pons M. et al., 1989). In the first step, a lumped chemistry model was used to calculate the flame shape, temperatures and hydrodynamics. In the second step, a detailed elementary reactions gas phase chemistry model or lumped kinetic schemes and detailed elementary reactions surface chemistry model or the here developed novel analytical treatment of surface process were used to calculate radicals and intermediates concentrations in the gas phase and at the surface, as well as growth rates. The simplified thermo-fluid sub-model used in the first step are both analytical and numerical in nature. In the latter case the combustion reaction mechanism is taken into account, while for the former the well known premixed laminar flame theory (Williams F.A., 1985) together with recent analytical treatments (Cremers M.F.G. et al., 2004 and 2007) is used to calculate the flame speed (*i.e.*, the laminar burning rate) and the velocity field.

As further simplification (exploited also for the 2-D approach), the chemical kinetics are neglected ("turned-off") because of the film diffusion limited regime. The growth rate is taken to be proportional to the gradient of the concentration normal to the wafer surface (which is proportional to Sherwood number) and, indeed, is given by the product of the local density, diffusion coefficient and the concentration gradient. For shake of brevity, the complete set of governing equations for each sub-model here considered are reported in here because it can be found elsewhere (Cremers M.F.G. et al., 2007). However, as generally in all forced convection problems, in order to obtain a better understanding of heat transfer process, study of

[2] local thermodynamics equilibrium model, where the thermochemical heat release is lumped into the effective gas mixture conductivity.

fluid dynamics of the fluid cannot really separated from the heat transfer aspects since the energy equation is dependent upon the momentum equation. Accordingly, the robust PREMIX code (PREMIX) is used as DNS tool to solve the full set of 1-D governing equations varying the gas-phase and surface chemical kinetic schemes adopted. What must be highlighted is that, the above mentioned numerical code permits to solve the system of ordinary differential equations by a separation-of-variables transformation (on the complete 3-D problem formulation) and, therefore, variables' radial distributions can be calculated. Nevertheless, as the authors recommend (Evans G.H. et al., 1996 and 1997; Chemkin-III manual), such a procedure, strictly speaking, is only valid for an unconfined infinite-radius disk and buoyancy-free flow. Moreover, only some boundary conditions are consistent with the transformation (*e.g.*, temperature, gas-phase composition and approach velocity all specified to be independent of radius at some distance above the disk). Summarily, the reliability of the *a priori* validation field is limited to "ideal" flow patterns. However, fortunately, the transformed equations generally still provide a very good practical approximation to the flow in a finite-radius reactor over a large fraction of the disk (up to ~90% of the disk radius) when the reactor operating parameters are properly chosen (*i.e*, optimized) and it was also proven that the computational results particularly matches experimental data for the thermo-fluid aspects (Winters W.S. et al., 1997(2); Joh S. et al., 1996 and 1997), although for noncombustion environments.

Finally, this approach (in its plug flow or 1-D-reduced formulations) permit to investigate the effects of buoyancy effects by means of the dimensional analysis. In particular, the so-called diagnostic factors ($G = gH^3/\upsilon^2$, $Gr_{\text{chamber}}/Re_{\text{in}}^2$ and $Gr_{\text{chamber}}/Re_{\text{disk}}^{3/2}$ (Vanka S.P. et al., 2004; Joh S. et al., 1997; Winters W.S. et al., 1997)) and the disk and wall mixed convection parameters ($Gr_{\text{wall}}/Re_{\text{in}}^2$ and $Gr_{\text{disk}}/Re_{\text{disk}}^{3/2}$, respectively (Winters W.S. et al., 1997)) are calculated and their values are compared to those achieved in
other combustion (Okkerse M. et al., 2000) and noncombustion (Santen H.V. et al., 2001) deposition reactor.

2-D model

As mentioned above, the set of 1-D flow equations, being derived by similarity transformation (Schlicting H., 1968 and references therein), are still valid for 2-D ideal flow model and, therefore, represent a valid aid in the understanding of the fluid paths developed in simple reactor configurations. In fact, if the typical width of the Bunsen flame cone is much larger than the target, and the angle of inclination of the stagnation flow is approximately perpendicular to the target surface, the stagnation surface can be considered flat within the radius of the stagnating jet. Therefore, as long as the jet flow acts as a plug flow, the impinging jet can be considered one-dimensional. Nevertheless, far away from the center axis (*i.e.*, outside the jet radius) two-dimensional effects become important, and the jet can not be considered one-dimensional. In fact, especially far away from micro-kinetic conditions, the opportunity to decouple the flow field and the energy transfer generally vanishes, particularly for two reasons: first, the velocity of unburnt mixture strongly influence the maxim flame temperature and can induce flame lift-off or flame extinction, and second, it is well known that the entrainment flow can strongly influence the flame strain rate as well as the maximum flame temperature, through its diluting action. Moreover, the complex fluid flow structures developed from confined or multi-nozzles configurations generally don't respect ideal flow patterns. In fact, despite the state of the surrounding gas mixture can be chosen arbitrarily (and, therefore, can be considered as a set of boundary condition for semi-infinite 1-D problems) for single nozzles (for both Bunsen and stagnation flow flame) or confined systems or MN burners it is governed by the conditions reached within the nozzle-to-target region and within the inter-nozzle zone, respectively. Accordingly, analytical treatments of the thermo-fluid problems are not performed for 2-D investigations. The above described two step procedure for 1-D model are here extended for 2-D problems and its results are compared to those obtained from the "ideal flow" (1-D)-reduced DNS ((1-D)-R-DNS) for single-nozzle configurations; while 2-D DNS are not performed (due to the higher computational effort, especially for Bunsen flame reactor).

From a modeling point of view, the effect of flow field is governed by the inlet and wall boundary conditions. In particular, in most of the calculations, all velocity components are safely assumed to vanish at the surface and the gas velocity at the nozzle exit is equally distributed over the cross section. The first approximation really represent the flow field developed near susceptor surface due to the jet dominated regime (*i.e.*, susceptor Reynolds number lower than jet Reynolds number). The second assumption is fulfilled to a high degree of approximation by most nozzles used technically. However, the case of laminar jets with fully developed parabolic velocity profile (Poiseuille flow) at the nozzle exit – when long tubes or rectangular ducts were used instead of nozzles – is here considered.

Furthermore, the here developed 2-D approach permits to gain insight the effects of fluid dynamics developed in the reactor. The flow in this type of reactors can occur either in the forced convection mode, where streamlines are curved but non-circulating above the susceptor, or in a mixed convection mode, with undesirable vortices caused by the heat release from the

flame front. The entrainment flow is governed by the flow rates and heat flux at the flame front(s), edges of the confined systems or at the susceptor surface. Moreover, it can dramatically affects the thickness uniformity of the deposited material and, therefore, are here computationally investigate for both single and multi-jet nozzle configurations. The complete set of 2-D equations together with the corresponding boundary conditions, numerically solved by the commercial COMSOL software.

The above defined common diagnostic dimensionless groups governing the mixing regime of the reacting mixture are calculated in order to compare our results to the 2-D fluid flow fields generally observed in 1-D. Nevertheless, although the mode transition can be roughly estimated by using this simple dimensional analysis (Evans G., 1987; Joh S. et al., 1996 and 1997), its results (and particularly the Re_{in}^2-dependence) could not hold where the flow field became three-dimensional as well as near instable flame conditions (flash-back, blow-off or extinction).

Furthermore, since the transport and chemical mechanisms are highly sensitive to the temperature distribution, it is necessary to include a description of heat transfer effects at system boundaries and therefore it is necessary to control the reactor wall and susceptor temperature distributions. In fact, the former affects the precursor deposit on the outer wall as well as the onset of buoyancy rolls near them, while the latter can influence the mechanism of diffusional transport through the well known thermal-diffusion effect. In this study, the standard idealized boundary conditions, fixed wall and surface temperature and adiabatic susceptor and reactor walls, and quartz wall case are considered. The isothermal wall approximation, implying some form of external cooling to maintain the walls at the temperature of the inlet gases, is used in most of the calculations reported in this paper because of the opportunity to cool the prototype reactor with an external jacket of cold flowing gas stream. Finally, for the third case here considered, the thermal boundary conditions take into account the radiation contributor, with particularly attention focused to its effects on temperature distributions in the boundary layer below the susceptor.

Because the effect of nozzle shape can be addressed through the principle of similarity (Bird. et al.,) the set of axisymmetric equations are not extended for plane geometry.

For MN burner, where an array of three multiple Bunsen flames are established below the susceptor along the radial coordinate, the same set of equations used to simulate the 2-D single nozzle Bunsen flame) are used. The main interesting features of this injector configuration is the opportunity to investigate different injection conditions, in terms of inlet velocity, inlet temperature and, in particular, mass flow rate distribution, as the generalized expression for the boundary conditions well evidence. The last of these three different boundary conditions (which can be interpreted as the precursor concentration distribution at fixed inlet velocity) is strictly related to the uniformity of the deposited material. In fact, multi-port injection represents an optimized strategy widely used in noncombustion metallorganic CVD reactors (Evans G.H et al., 1988).

The performance of confined systems with MN burner are optimized by varying the center-to-center nozzle separation distance in order to investigate, firstly, the temperature profile (or, alternatively, the thickness of the thermal boundary layer) and secondly, the effect of concentration profiles. Nevertheless, because of the stretching action of shroud flows, carefully attention should be devoted to flame stability, although the 1-D seems to computationally prove the stability of the flame front under the here considered operating conditions. In fact, the 2-D decoupled model permits also to investigate effect of stretching action on thermo-fluid problems for burner-stabilized (or rim-stabilized), lifted or substrate stabilized flame.

Finally, for both 0-D and 1-D models, particular attention is focused on our novel analytical treatment of heterogeneous surface kinetic schemes and on the impact of the multicomponent mass transport algorithms.

Multicomponent transport algorithms

For 0-D model the gradient appearing in the definition of diffusional velocity in each transport algorithm are approximated accordingly to the thin film theory and the adopted multicomponent diffusion model is the classical Fickian approach further simplified under the Wilke approximation (Wilke C.R., 1950). In order to ensure mass conservation, all species fluxes except one are calculated in this way. The remaining species, with the largest mass fraction (*i.e.*, H_2), is calculated from the constraint that all diffusion fluxes should sum up to zero. The main features of the remaining three models here considered (Fortran CHEMKIN-III transport library) are well summarized in the Chemkin manual, indeed nowadays permit, at moderate computational cost, in situ calculation of all the necessary transport coefficients of gas mixtures using rigorous and accurate expressions.

Chemical kinetics mechanisms

The here adopted detailed gas phase kinetic schemes for the deposition process follow the same framework well described in Cavallotti et al. (Cavallotti C. et al., 2001). Because of the operating AP conditions, the fall-off effects (*i.e.*, the dependence of the kinetic constants on the gas pressure) are carefully taken into account for unimolecular reactions. Moreover, for both silane and chlorosilane routes, the highly exothermal heat of combustion together with the high concentration of HCl results in the formation of the expected growth-driven precursor species (mainly SiH_2 and $SiCl_2$) and govern the amount of the undesired tetrachlorosilane species ($SiCl_4$) as well as the etching effects (here considered in both lumped and detailed surface kinetic schemes).
Despite of surface chemistry of silanes and chlorosilanes can be considered to be well represented by the kinetic schemes reported in Cavallotti et al. (Cavallotti C. et al., 2001), our novel analytical treatment of heterogeneous surface kinetic mechanism for $SiHCl_3$ deposition permits to simplify the kinetic schemes placing itself as an advance in the modeling of kinetic surface processes. In particular, under the assumption of pseudo-steady state (PSSA) for adsorbed H, SiCl and Cl species and negligible site coverage fraction for these first two species, the following analytical polynomial expression results (rigorous derivation can be given under request to the author):

$$\alpha\left[\mathrm{Cl}^{*}\right]^{4}+\beta\left[\mathrm{Cl}^{*}\right]^{3}+\gamma\left[\mathrm{Cl}^{*}\right]^{2}+\delta\left[\mathrm{Cl}^{*}\right]+\theta=0, \qquad (1)$$

where the four coefficients depend on the kinetic rate constants of the reactions constituting the simplified kinetic mechanisms. In particular, the term α represents the effect of HCl and $SiCl_2$ desorption (increasing as the desorption rate constants increase), while the others are non-linear expressions of the kinetic rate constants coupling together different surface processes (adsorption, desorption and surface reaction).
Eq.(1) admits an analytical solution[3] and its cubic term are not negligible for an exact computing of the number of free coverage site. Finally, what must be highlighted is that all the surface reactions involved must be considered only in the forwards directions.
Relative to the flame chemistry, the reaction mechanism is chain in nature because the reactions proceed through the active intermediates Cl and H, which are regenerated as the reaction progresses. In this work, two different kinetic schemes are adopted: the well known five-step mechanism (lumped model) reported in Copperstbwaite et al. (Copperstbwaite D.P. et al., 1991) and the more detailed one recently proposed by Leylegian et al. (Leylegian et al., 2005).
As concluding remark we observed that the complex temperature and pressure dependences of most of these reactions were parametrized in a Troe form (Gardiner W.C., 1984), which uses three parameters each to describe the rate constants at the high-pressure and low pressure limits, plus four additional parameters to describe the scaling of the rate constant with pressure.
For shake of completeness, the complete set of reactions are reported in Tables 1-3.

Sensitivity analysis

The here developed 0-D and 1-D local parametric sensitivity analysis permits to individuate the precursor species which play the major role in the deposition rate under a wide range of operating conditions. In particular, the effects of inlet flow rate V_{in} and susceptor temperature T_s are here considered. As natural choice, the growth rate is taken as objective sensitivity, while the inlet flow rate and temperature are the two model input parameters.
What must be highlighted is that the gas phase temperature (*i.e.*, the second component of the parameter vector $\boldsymbol{\Phi}$) influence the mass fluxes vector $\boldsymbol{M}$ (which is can be easily calculated from the model solution vector $\boldsymbol{y}$) because of the temperature dependence of both the diffusion coefficient matrix and the thermal diffusion factor. Moreover, the change in the temperature gradients established below the susceptor also affect the components of the vector $\boldsymbol{M}$. Therefore, in order to better understand the species which are subject to the major transport fluxes, the (normalized) objective sensitivity are also calculated as (normalized) change in mass fluxes vector due to gas temperature variation.

Results and Discussion

[3]Gerolamo Cardano, *Artis Magnae sive de regulis algebraicis*, 1545.

As stated above, because of the lack of experimental data, the model validation cannot be checked by direct comparison with reliable experimental results. Accordingly, direct comparisons between the predicted results for different (0-D, 1-D and 2-D) models are addressed in order to highlight the individual contributions to the overall computational optimization strategy. In particular, the here present discussion is focused on the effects of operating conditions and reactor design parameters (reactor geometry and configurations) on the process performance (in term of growth rate uniformity and productivity). Two dimensionless variables, introduced by Vanka et al. (Vanka S.P. et al, 2004), that are directly related to the economical benefit of the process, are introduced as process diagnostic factors: the so-called usage (*U*, fraction of precursor that reacts at the surface[4]) and the precursor utilization efficiency (η_P, the fraction of the precursor atoms or molecules that are incorporated into the film). In fact, as Vanka et al. highlighted (Vanka S.P. et al., 2004), optimizing η_P and *U*, may result in substantial cost savings, although significantly less attention have received to them in the available literature. What must be noted is that, although these two factors address different aspects of the process (and, indeed, the former represent the ratio of the mass of silicon precursors deposited on the whole surface to the mass sent through the nozzle, while the material growth can be more rigorously represented by the latter!), for diffusion limited regime these two parameter assume the same physical meaning. Moreover, the more explanatory rector yield (*Y*) are calculated as the ratio of the mass of silicon sent through the nozzle to the mass deposited on the whole surface.

Effects of operating conditions

The effects of the following operating conditions are particularly here addressed: inlet flow rate, feed stream composition and imposed temperatures at susceptor surface or at reactor wall.

For each nozzle configurations, the Reynolds number Re_{in} (based on the nozzle exit diameter and the mean velocity, viscosity, and density of the gas at the nozzle exit) is of the order of 10^2-10^3 (laminar flow regime). The Reynolds number in the flame front Re_{flame} based on the typical flame cone width, laminar burning velocity, viscosity and density in the flame front is of the order of 10^2. Nevertheless, even if the fluid regime is laminar, relatively high Grashof number (*i.e.* up to 10^2-10^4) can be reached due to the effect of the heat release from flame front.

The results of 0-D model simulations are shown in Figs. 4-6 and Table 4. Under the here considered operating conditions, the calculated maximum gas-phase temperature are close to the adiabatic flame temperature[5] (which can be easily calculated from classical thermodynamics) and, thus, the thermo-fluid flow aspects depend only on the imposed operating conditions at reactor inlet (inlet flow rate, feed stream temperature and composition), at susceptor surface (susceptor temperature) and at reactor wall (isothermal or adiabatic conditions). The asymptotes of the diffusion limited growth curves reported in Figs. 4 and 5 well evidence that increasing the flow rate appears to be quite advantageous, due to the enhancement of the both convective and diffusional mass transfer rate. In fact, the molecular diffusion (*i.e.* the ordinary binary diffusion coefficient) depends on the adiabatic flame temperature, which indeed increases with increasing the flow rate[1]. The mass transfer rate also non-linearly increase with the inlet velocity as the dependence of the Sherwood number on the Reynolds clearly predict. Moreover, the relative contribution of these two mechanisms on the overall growth rate can be investigated by varying the Péclet number (which is usually in the 10^1–10^2 interval values). The same qualitative trends are still obtained for kinetic limited regime and, as the slight change in the slope of the asymptotic kinetic limited curves, the effect of reactor residence time (in the magnitude order range of 10^{-4}–10^{-5} s) don't dramatically affect the deposition rate under this regime. Furthermore, the inlet mixture composition can affect the growth rate and the here presented results suggest to use silicon precursors' inlet (H_2-based) volume fraction higher than 19% (vol.) to achieve moderate growth rate (*i.e.* higher than 1 μm/min) for both silane and chlorosilane routes. In fact, at lower temperatures, where the process is reaction-controlled, the relative abundance of SiH_4 ,$SiHCl_3$ and the conversion of SiH_2 and $SiHCl_3$ to Si_2H_6 and $SiCl_2$ by the gas-phase reactions (G2) and (S1) respectively, limits the deposition process, while as the temperature increases, the relative concentration of SiH_2 (which has a surface reactive probability of almost unity) and $SiCl_2$ is increased. In fact, the calculated superficial compositions of the main growth-driven species (SiH_2 and SiH_4, for silane route, and $SiCl_2$ and $SiHCl_3$, for chlorosilane route) increase of about a factor of five varying the inlet molar fraction of $SiHCl_3$ from 1 to 15 %. All these considerations well agree with the well established theory on the physical mechanisms governing CVD processes. In fact, a slowly increase in the growth rate is predicted until the gas phase temperature below 1600 °C is reached and then further increase in the temperature brings the systems from film diffusion limited to kinetically limited, reproducing the well known qualitative trend generally referred as Arrhenius's plot. Moreover, the opportunity to cover the a wide range of operating temperature and precursor inlet concentrations (encompassing both reaction controlled and diffusion-controlled deposition regimes) also highlights the robustness of this simplified approach.

Notably, the 1-D model results well agree with the 0-D ones, as a direct comparison between the of growth rate at stagnation point (reported in Figs. 10) and the growth rate calculated from the 0-D model well evidence. Moreover, this agreement is also still valid for the precursor surface compositions (Table 4), the maximum flame temperature and the optimized (in term of maximum growth rate) oxy-fuel volumetric flow ratio.

However, the main advantages of the 1-D model is the opportunity to computationally investigate the flame and impinging mixture properties along the axial coordinate. In fact, the axial temperature and velocity profiles reported in Fig. 9 show

---

[4] $U = \frac{\int_{A_w} \rho D \, \partial Y/\partial \xi|_w dA_w}{\int_{A_w} \rho v_z^{in} Y_{in} dA_w}$, from Vanka et al. (Vanka S.P. et al, 2004).

[5] data not shown for shake of brevity.

that there exists an interval values for the inlet gas flow rate, where the flame may be stabilized in the stagnation-point flow above the substrate and an increase in flame stretch by increasing flow velocities to near extinction results in a substantial increase in growth rate. As an example of the simulation results, under the usually inlet flow rate value of 10 slm, the peak strain rate of ? s^{-1} occurs 0.1 cm above the substrate, which may be taken as the velocity boundary layer thickness. The thermal boundary layer is seen to be somewhat thicker, with the temperature maximum occurring 0.3 cm from the substrate. From Fig. 9 it is evident that for velocities greater than 15 cm/s (*i.e.* about 17 slm), the flame is lifted from the nozzle exit and stabilized by the substrate surface, as the steep temperature rise a few millimeters below the target surface well evidence (pick line in Fig. 9). Under these conditions, the flame is stabilized on the substrate surface, allowing the inlet gas velocity to exceed the adiabatic flame speed of the mixture, while the maximum flame temperature (always close to the adiabatic flame temperature) is slightly reduced. As expected, the deposition rate at stagnation point increases with increasing (at fixed inlet precursor composition) inlet velocity (Fig. 10). Moreover, as the strain rate is increased almost linear increase in growth rate is computationally observed. Notably, 1-D trends well quantitatively match 0-D model trends reported in Fig. 6 and, thus, are not reported here for shale of brevity. Moreover, as the flame is pushed closer to the stagnation surface (*i.e.* increasing the inlet flow rate), the numerical solution diverge.

It is generally known that in the neighborhood of the extinction point computation of the solution often becomes difficult. In particular, at the extinction point the Jacobian of the system often becomes singular. Accordingly, the here results seems to suggest that flame extinction roughly occurs for unburnt mixture velocities around 70 cm/s. Nevertheless, more in depth study must be surely performed in order to understand the exact mechanism leading to flame extinction. In fact, in a wide number of cases, it was found that the Lewis number played an important role in the behavior of these flames near extinction.

Moreover our results clearly show that the effects of operating conditions not only on the thermo-fluid fields but also on the growth rate and concentrations fields can be adequately investigated by means of 1-D decoupled as well as DNS approaches. Moreover, as Cremer's and co worker demonstrated for impinging flame jets (?), the comparison in Figs. 9 highlight that the analytical velocity and temperature distributions, calculated for the potential core and the post-flame regions, agree with the numerical simulations.

The results of 2-D model permit also to gain insight on the dependence of the thermo-fluid fields from the operating conditions and, therefore, to better optimize the reactor performance even for axisymmetric single-nozzle configuration. For small values of the mixing parameters ($\mathrm{Gr}_{\mathrm{chamber}}/\mathrm{Re}_{\mathrm{disk}}^{3/2}$, $\mathrm{Gr}_{\mathrm{chamber}}/\mathrm{Re}_{\mathrm{in}}^{2} < 10^{2}$) as well as for value of the mixing diagnostic factor G lower than 10^{3} no flow recirculation are observed above the rotating susceptor. However, the inlet gas velocity is an additional parameter governing the entrainment effects through the specification of the flow boundary condition. The curves reported in Figs. 10-15 confirm that varying the gas flow it should be possible to bring about a proper balance between the forced flow and the entrainment paths and hence to achieve a better approximation to a uniform deposition rate.

In fact, for burner stabilized flames, the recirculating cell can be eliminated by increasing the inlet flow rate and such a solution also improves film uniformity considerably (Figs. 10 and 15), as many studies in the noncombustion environments seems to suggest (Fotiadis D.I. et al., 1990; Kuijlaars K.J. et al., 1996; Vanka S.P. et al., 2004). Moreover, the maximum growth rate (reached nearly close to the stagnation point) is enhanced by increasing the inlet flow rate (Fig. 10 and 15), similarly to results obtained by 0-D model and 1-D DNS, although in terms of general trend than numerical matching. Moreover, the curves plotted in Figs. 10 well highlight that, over the inner half of the disk (within the stagnation region), the 2-D deposition rate is uniform and identical to the (1-D)-R-DNS. Nevertheless, moving along the radial coordinate a decrease in *GR* is calculated, while approaching the susceptor edge the further increase in *GR* is the results of the flow acceleration and the change of flow direction from radial near the disk to axial in the annular outflow region.

As the analogy between heat and mass transfer suggests, all models including buoyancy effects (2-D decoupled approach) yield lower values for heat flux at the stagnation point than identical models neglecting buoyancy (1-D and (1-D)-R-DNS approaches) and, as the system flow rate increases, the sensitivity of the uniformity to buoyancy effects decreases (Fig. 10). In fact, by increasing the turbulence level and decreasing the temperatures within the chemical equilibrium region of the flame, the dilution effect of any entrained flow would decrease the transfer fluxes within this region (Fairweather M. et al., 1984) and explain why 1-D models results overestimate the stagnation point growth rate. Moreover, as it is clearly shown in Figs. , the flame properties dramatically depend on the stretch rate, which is governed by the inlet flow rate distribution. In particular, although the maximum flame temperature (reached closely near the flame tip) seems to be quite insensitive to the inlet flow rate for burner- or rim- stabilized configurations, its value drastically shoots down (especially for Bunsen flame) with increasing the flow rate due to the major role played by heat transfer release mechanisms (front flame front) governing the lift-off flame stability (Figs. 13). Furthermore, although the physical trends for growth rate vs. inlet velocity are calculated through 2-D simulations well match the (1-D)-R-DNS for flames weakly lifted-off from the burner nozzle, 2-D model results in lower growth rate (especially at susceptor edge) for highly lifted Bunsen flames (Fig. 18). Nevertheless, especially for Bunsen flames, the main advantage of lifted configurations is the increase in uniformity at expense of the growth rate, as the equi-concentration lines reported in Figs. 11, 12, 14 and 15 well evidence.

A parabolic velocity profile at the inlet enhances the transport of precursor to the surface near the center of the susceptor, and reduces the transport further out, as a result, uniformity is greatly reduced, though precursor utilization efficiency η_{P} slightly increases (from 25% to 30%) since the bulk of the deposit occurs at the center, and less precursor gas is lost as it

bypasses the substrate. Notably, on the contrary, the premixed flame structure seems quite independent on the flow rate distribution imposed at burner nozzle exit (*i.e.* mean centerline velocity less than 5 cm/s) even at moderate inlet velocity.
Furthermore, the results of 2-D model clearly show that (Fig. 18), for precursor concentration uniformly distributed along the inlet single nozzle diameter, precursor utilization efficiency increases linearly – within the interval value between ± 20% of the here calculated optimum operating conditions – with growth rate, since the enhanced growth rates at a fixed mass flow rate of precursor necessarily result in higher efficiency. However, efficiencies are fairly low, typically less than 40%, with the remaining 60% bypassing the substrate and proceeding out the exhaust. Separation and recycling can potentially recover some of this (but only with added cost!).
The effects of the inlet concentration profile for various flow rates is a relatively simple 2-D problem since the concentration field is passive to the flow and temperature fields (Figs. 11, 12 and 14). Nevertheless, controlling the inlet concentration is more difficult than increasing the inlet flow rate or adopting MNC, as already Cho et al. (Cho W.K. et al., 1999) noted for noncombustion CVD. Moreover, as our results (Figs. 16) clearly show, the former solution permits to achieve uniform distributions of precursor gas near the susceptor only for small "standoff" distance and for stagnation flow flame (*i.e.* porous burner). In fact, the 2-D concentration field, reported in Figs. 12c) and 14 – corresponding to the unoptimized reactor conditions – shows that the equi-concentration lines near the wafer surface deviate much from the parallel to the surface position. This results in non-uniform normal concentration gradient distribution along the wafer surface and, consequently, the non-uniform deposition rate. In fact, even under inlet flow rate higher than 15.0 slm value near 10% of thickness non-uniformity still persist (Figs. 10 and 15), especially for Bunsen flames (Fig. 15). On the other hand, the equi-concentration lines obtained through the optimized multi-nozzle configuration (Figs. 11c) and 14) become nearly parallel to the wafer surface. Nevertheless, as Fig. 14 well evidences, for Bunsen flame the step concentration gradients (which faithfully follow the streamlines[6]) cannot be moderate only by adjusting the operating conditions, but the addressing of reactor geometry (and in particular the "standoff" distance) become necessary in order to optimize the uniformity of the deposited material.
For MN burner, the stretching action of the uniform outer-flow (shrouding the premixed flame front at moderate flow rate (*i.e.* 3 slm)) seems to flatten the flame front at negligible expense of the flame stability. It's interesting to note that when the precursor concentration in the shroud flow is increase from 5% to 10%, while the inner flow rate is kept at 8 slm, the uniformity of the concentration field for the growth-driven precursors above the surface is increased, because the higher velocity o the shroud stream facilitates the increased mass transfer of them to the outer stream by diffusion towards the reactor wall in the downcoming part of the shroud flow. Therefore, the flow patterns developed in this reactor as well as the flat flame front established in front of the susceptor (Fig. 19), brings the precursors closer to the surface and, accordingly to the results obtained for single nozzle configuration, increasing the inlet flow rate (at fixed inlet concentration) the stagnation point growth rate is also increased. In fact, for the optimized multi-nozzle configuration (Fig. 18,thin blue line), precursor utilization efficiency increases greatly (up to 52%), exceeding 25% for the optimized stagnation flow flame configuration (35%).
Comparison of the streamlines and isotherms for some cases discussed above (Fig. 11,14 and 17) suggest that, especially for stagnation flow flames or MNC, the susceptor temperature distribution has no significant influence on the flow and temperature fields in the gas phase under the here considered conditions (*i.e.*, 750K < T_s < 975 K and 0.8 atm < P < 0.9 atm). In fact, even at low flow rates corresponding to Re_{jet} =20 fully developed thermal boundary layer profiles for substrate temperatures at or below 800 K are calculated. Moreover, it's interesting to note that for higher substrate temperatures (*e.g.*, 1400 and 1600 K) the 1-D cannot be sufficiently described by the similarity transformation: for a specific flow rate, the thermal boundary layer profiles above the substrate don't collapse onto a single curve and the solution of the 1-D problem diverges. On the contrary our decoupled approach predict growth rates lower than , in agreement to 0-D model results reported in the Arrhenius' plots (Figs. 4-6).
However, what must be highlighted is that the optimized MN burner seems ensure flat radial temperature profiles (around about 1000 K) close to the substrate surface (Fig. 17a)).
Furthermore, the model results present weak sensitivity to the effect of reactor wall heat transfer conditions (isothermal or adiabatic wall) – within the here considered reactor operating conditions. In particular, the 2-D simulation for unoptimized reactor configurations (Fig. 20) clearly shown, the hot wall causes the incoming or burnt gas to expand, but the result is only a natural convection cell next to the reactor wall. Moreover, compared to an adiabatic wall, the cooled isothermal wall boundary conditions allow a larger value of the Grashof number to be employed without recirculation. What must be note is that these results seem to reflect the general trends obtained by many other authors for noncombustion environments (Vanka S.P. et al., 2004; Fotiadis D.I., 1987).
The 1-D concentration profiles (Figs. 6-8) and the 2-D equi-concentration lines (Figs. 11,12,14,17) well agree with the results of many other works, in terms of SiH_2 molar fraction distribution. Because SiH_2 is nearly close to equilibrium when gas phase temperature exceeds 1300 K, its composition depend on the temperature fields (rather than on its dissociation rate). In fact, it's well evident in Figs. 11 and 17 that its concentration fields are (almost exactly) congruent to the temperature ones and, notably, this consideration are valid for both rim stabilized or lifted-off flames and stagnation flow or

[6] not reported here for shake of brevity

Bunsen flames confirms. The vapor phase molar fractions for $SiHCl_3$ and $SiCl_4$ species have about the same magnitude order, in accordance to the stoichiometry of the overall $SiCl_4$ production reaction suggested[7].
Relative to the flame chemistry, the model simulations show that, under high fuel to oxidant ratio conditions (*i.e.*, Cl_2 as reaction limiting agent), the burnt flow is nearly an equimolar H_2-HCl mixture, as the stoichiometry of the overall combustion reaction suggests.
Finally, we need to highlight that, the optimization of the reactor performance cannot be based only on the operating conditions, but a proper design of the reactor geometry and configuration must be addressed. For example, the entrainment effects are dramatically sensitive to the standoff distance, as the poor uniformity achieved for chamber height larger than 8 cm (even if the inlet flow rate is increased up to 35 slm) clearly suggest.

Effect of reactor design parameters
For the 0-D model, the effect of reactor geometry and configurations are lumped within two input values: the reactor volume and the susceptor dimension. Therefore, the conclusions above addressed about the effect of inlet flow rate are still valid here, accordingly to the concept of reactor residence time (*i.e.* the ratio between the reactor volume and the inlet flow rate). In fact, by increasing the inlet flow rate (at fixed inlet composition) or by increasing the specific deposition area (*i.e.* the ratio between the susceptor area and the reactor volume) similar results are obtained[8]. Nevertheless, higher order model are necessary in order to optimize the values for the key geometric parameters governing the process performance.
The first key parameter here considered are the so-called "standoff" distance (H) between the nozzle exit and the susceptor – also named here chamber height or separating distance. In fact, controlling the flow path of the precursor gas can be effective by either altering the chamber shape, which indeed has a considerable impact on the existence of natural convection driven recirculation since this distance enters into the Grashof number as H^3. Thus, strong recirculation cells are expected to exist in tall reactor configurations while the cells will disappear as the reactor is shortened. Accordingly, a reduced chamber height can minimize the entrainment of the carrier gas to from the environment and, thus, secondary flows cannot be readily established. The confinement of the flow in the narrower channels results in higher mean velocities, and these appear to convey the buoyant recirculation regions downstream to regions in which there is no effect on the deposition (Figs. 11); a behavior also observed in noncombustion environments (Vanka S.P. et al., 2004). The enhanced interface abruptness due to the reduced residence time of the reactants over the substrate, improves thickness uniformity and increased process parameter window due to the insensitivity of growth uniformity on the above optimized operating conditions. On the contrary, as the standoff distance becomes larger, the mixing due to diffusion dominates and a uniform concentration profiles near the susceptor cannot be established (Figs. 12 and 14).
Nevertheless, because of the flame stretch, the optimization must take into account the undesired (and dangerous!) effects of short chamber height, which may lead flame blow-off, extinction, flashback or pre-heating of the inlet mixture. In particular, due to the lack of experimental data, the simple dimensional analysis approach suggest to safely settle the lower limit of this geometric parameter to 1.0 and 1.5 the for Bunsen and stagnation flow flames, respectively.
For the single nozzle configurations, the results of 1-D and (1-D)-R-DNS approaches provide valuable trends and aid in interpreting the more complex results of the 2-D calculations presented later. The Figs. 17 illustrate the strong dependence of the growth rate distribution along the wafer radius on the standoff distance. Our results show that it is necessary to lower the aspect ratio *AR* down to 1.0 in order to mitigate the effect of cold flow recirculation. In particular, unoptimized configurations (Fig.12 and 13a),b),c)), leads to undesired non-uniformity in the boundary layer thickness near the stagnation or at outer edge, due to an improper balance between the buoyancy and the forced momentum.
On the contrary, the optimized configuration (Figs. 11 and 13d)), due to its small aspect ratio, is forced convection dominated and, therefore, the film thickness decreases away from the center of the wafer, except near the edge due to the bending of the flow. Moreover, the 2-D simulations permit to set the transition value for the dimensionless diagnostic factor G (for inlet flow rate within the 1-10 slm interval value) around 10^3, below which the flow is forced convection dominated. Based o.n these results, it can be concluded that either too small or too large gap distances can lead to flame instability or uniformity problems in stagnation flow reactors, respectively.
Furthermore, the comparisons between the results reported in Fig. 15 and 16 clearly show that the growth rate strongly depends on flow parameter ($FP = Re_{\text{in}} / \sqrt{Re_{\text{disk}}} = 2r_{wall} \left|\overline{v_z^{in}}\right| / r_{disk}\sqrt{\upsilon^{in}\omega_{disk}}$) and Re_{disk} a much greater extent at smaller aspect ratios ($AR \equiv H/r_{\text{disk}} = 0.5$) than at larger spacings (AR = 2.5). Although the similarity solutions are valid for infinite radial extent values of R_{disk} = 40 cm and R_{wall} = 45 cm are used here in the calculation of the dimensionless parameters *AR*, *FP*, and Re_{disk} to facilitate comparison with the 2-D results. Fig. 10 shows that the growth rate distribution increases approximately linearly with *FP* for both values of *SP*. Moreover, the their variation with *FP* is much larger for smaller value of *SP*. For both values of *AR* and for fixed inlet velocity (10 cm/s), GR decrease with increasing Re_{disk} (Fig. 17) while reach an asymptotic value that is equal to the deposition rate an infinite rotating disk at $Re_{\text{disk}} \approx 400$. Moreover, the 2-D results in Figs. 10 show that the effect of inlet velocity on the radial variation of the deposition rate is greater for larger value of *AR*. Once again, for all case here considered, the results obtained from the 2-D decoupled approach well match with the (1-D)-R-DNS[9].

[7] $SiHCl_3 + HCl \leftrightarrow SiCl_4 + H_2$.
[8] not reported here for shake of brevity
[9] direct comparison are not shown fo shake of brevity

By comparing the equi-concentration lines and isotherms (plotted in Figs. 11,12 and 14) and the corresponding growth rate distributions (Fig. 16), the first general comment that can be made about these 2-D results is that for each optimized configuration the concentration field of the main growth-driven precursors near the deposition surface
Even if it is well known that in order to improve uniformity it can be advantageous to increase the size of the inlet so that reactants are distributed over a wider substrate area, flame stability impose a narrow range for this geometric parameter. Therefore, in the here considered calculations for single nozzle configuration it is varied within the 1-4 cm interval value. However, widening the inlet nozzle diameter for MNC appears to improve uniformity with small efficiency penalties and at negligble expense to the flame stability (Figs. 18).
For the case of MNC, in order to avoid flame flashback, the single nozzle diameter is fixed to 1.5- cm while the adjustable geometric parameter governing the uniformity becomes the center-to-center separation distance (*d*). The optimal value for *d* is the maximum inter-nozzle distance that yields good film uniformity. In fact, as mentioned above for MNC, the precursor utilization efficiency are doubled with respect to the single nozzle reactor and, thus, our attention should be focused on the flattening of the thickness distribution, instead of increase the local surface concentration. Fig. 17 shows, for the optimized reactor configuration, the velocity, temperature and concentration fields. As it's appear evident, the presence of small recirculating paths within the inter-nozzle preflame region don't negatively affect the growth rate distribution, but it represents a huge advantage. In fact, because of the higher degree of mixing achieved within the zone delimited by the two flame fronts and the susceptor surface, the standoff distance can be increased (of about 25% with respect to its reference value) at negligible expense of the thickness uniformity.
Furthermore, it is generally accepted that making the susceptor rotate can also improve the growth rate and its uniformity as the centrifugal force enhances the inflow of the new reactant gas by throwing the used gas outward. As the rate of rotation increases (up to 500 rpm) the growth rate (especially near the center) increases due to the centrifugal pumping that pulls the gas towards the spinning disk along the axis of rotation and throws it out at the perimeter of the disk. The growth rate increases with rotation because of the viscous pumping caused by the rotational forces and the resulting thinning of the boundary layer (Fotiadis D.I. et al.,1990). The pumping action of the spinning susceptor creates a downward flow that breaks the natural convection driven recirculation cell and establishes a force convection dominated flow. However, although the film uniformity and growth rate can also be increased, the onset of the typical finger-shape roll at the edge of the distribution curves is not present up to 200 rpm (Figs. 16). Moreover, in Figs. 16 and 18 it is evident that increasing the aspect ratio dramatically reduce the role played by the fluid paths induced by susceptor rotation. In fact, susceptor disk rotation alone cannot counteract buoyancy effects, as Vanka et al. already noted for noncombustion CVD reactor (Vanka S.P. et al, 2004), and especially for standoff distance greater than 5 cm, its influence on the boundary layer thickness can be neglected, due to the stronger effect of recirculation paths. In fact, as it has been above demonstrated, for such unoptimized conditions only MN burner can effectively increase the process performance.

Impact of kinetic schemes
Notably, the novel analytical and the detailed surface mechanisms of Cavallotti et al. (Cavallotti C. et al. 2001) begets similar results even if better in terms of growth rate (Fig. 4-6) than superficial composition (Table 4) over a wide range of operating conditions and independently to the model in which they are implemented. This seems to confirm the advance of the here proposed treatment of surface process reducing the computational effort in modeling silicon deposition via chlorosilane route.

Impact of multicomponent mass transport algorithms
It is well-known (Dollet A. et al., 2004) that thermal diffusion tends to separate species of different size and molecular weight, heavy molecules moving towards cold regions whereas light molecules move towards hot regions. The high temperature and concentration gradients nearly-normal to the Bunsen flame fronts seems to suggest that the heavy precursor species ($SiCl_2$, $SiHCl_3$, Si_2H_6 and SiH_2), due to its similar molecular weight, can move towards the cold walls and therefore for them more non-uniform 2-D profiles at the substrate are expected with respect to those of the light H_2 and HCl species, in accordance to the Soret mechanism. Indeed, the mass fraction profiles presented in the Figs. ? relatively well agree with this consideration. Moreover, Model simulations assuming only Fickian diffusion overshoot the plateau region (of the Arrhenius's plot) calculated by including the Soret diffusion term (Figs. 4-6), as Coltrin and coworkers (Coltrin M.E. et al., 1996; Kleijn C.R. et al., 1991) suggested. Nevertheless, the higher deviations observed by Coltrin and coworkers (deposition rates were approximately up to 50% higher without thermal diffusion in the model for inlet conditions of 0.7 torr SiH4 in 624 torr of carrier gas, either hydrogen or helium) are not obtained under the same gas phase and susceptor temperature, pressure and inlet flow rate operating conditions.
Nevertheless, as previously mentioned, only the sensitivity analysis can permit quantitatively validate this finding.

Parametric sensitivity analysis
Finally, in Fig. 19 it is shows how normalized objective sensitivity (mass fluxes) of the most important species depends on the susceptor temperature. It's evident that multicomponent algorithms neglecting and including Soret effect have dramatically impact on the surface composition vector ($\boldsymbol{y}^{\mathbf{sup}}$), particularly for susceptor temperature above 1300 K. The solution of the corresponding model system also highlight that for concentrated silane inlet mass fraction, the deposition rate computed with Soret effect can be about 30% less. Therefore, such an approach are highlighted as only an in depth

treatment of model parametric sensitivity can quantify the contribution of parameter, which are not evident through a first “heuristic” investigation.

Summarily, for a relatively wide range of reactor operating conditions, the simplified 0-D model yields results that are in quantitative good agreement with 1-D and 2-D ones. Nevertheless, higher order models (containing detailed multicomponent mass transport algorithms) is necessary for the optimization of the reactor geometric parameters in terms of process productivity and deposited material quality.

List of Figures

Refs. to Masi t al. (Masi M. et al., 2003, 2001, 2002) for Figs. 1,2,3

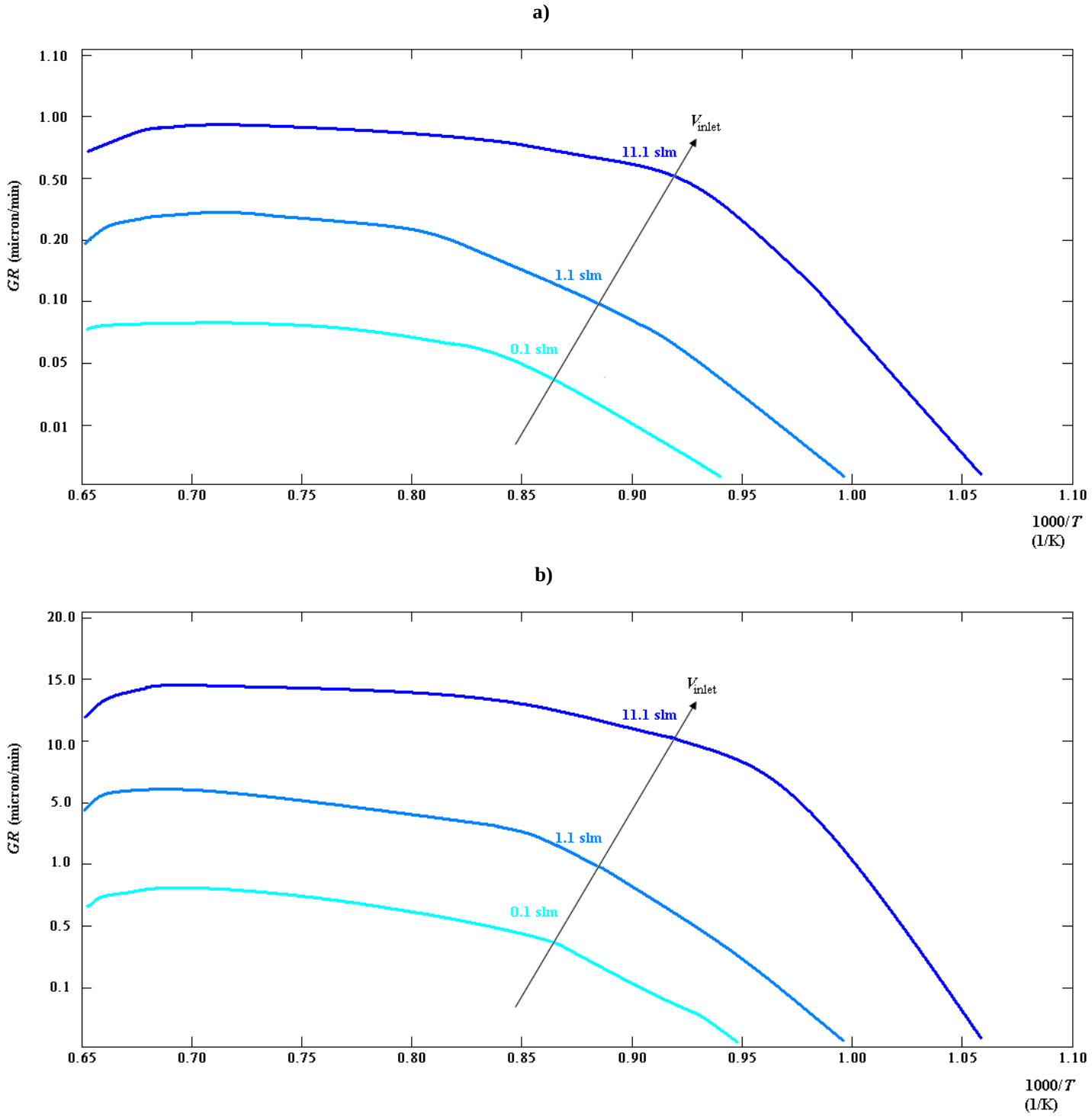

Fig. 4 – Arrhenius's plots for the effect of inlet flow rate on the (0-D model based) predicted silicon growth rate under **a)** dilute, $SiH_4/H_2 \approx 1\%$ vol. and **b)** concentrated, $SiH_4/H_2 \approx 19\%$ vol., inlet precursor compositions.

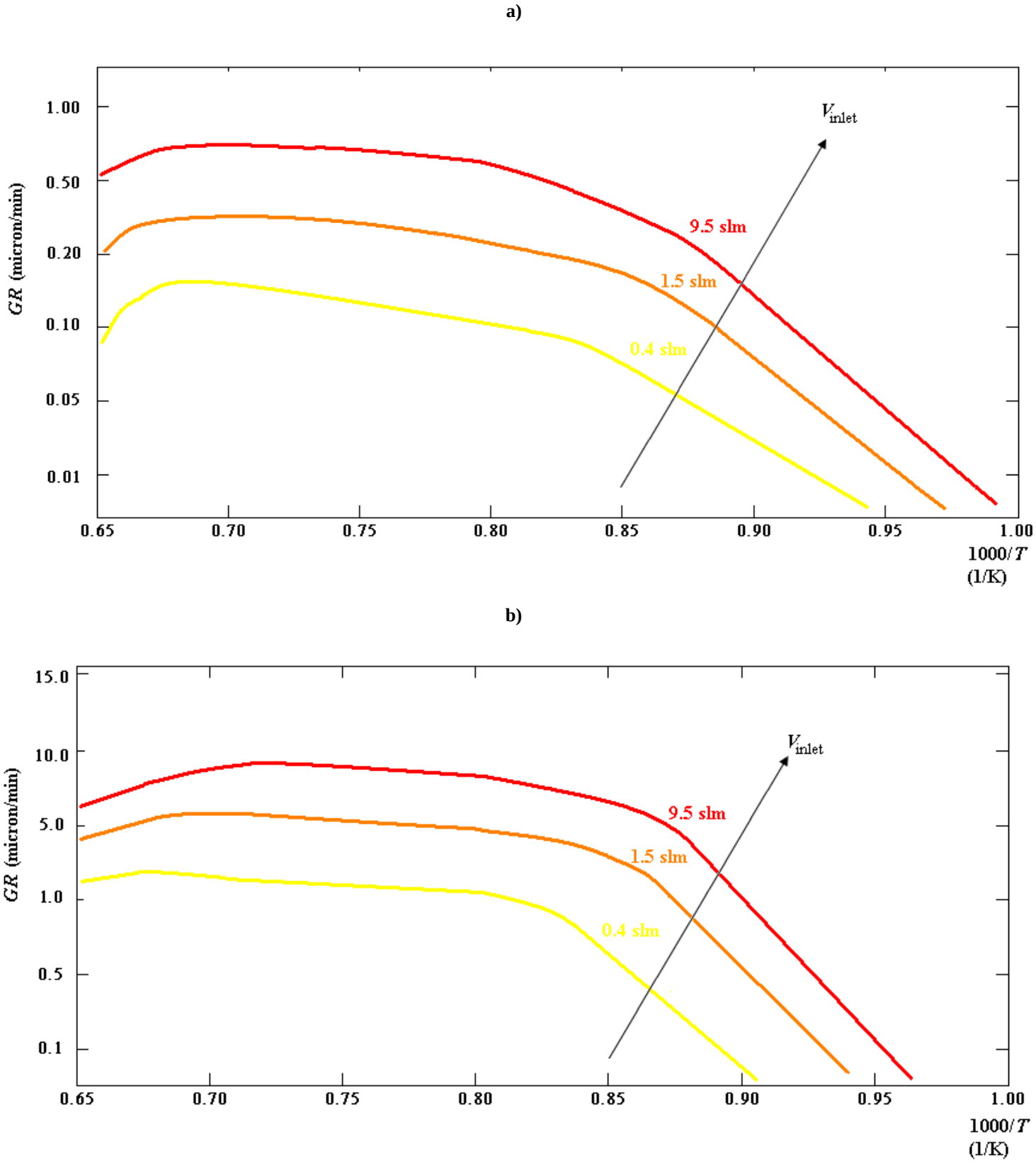

Fig. 5 – Arrhenius's Plot for the effect of inlet flow rate on the (0-D model based) predicted silicon growth rate under **a)** dilute, $SiHCl_3/H_2 \approx 2\%$ vol. and **b)** concentrated, $SiHCl_3/H_2 \approx 15\%$ vol., inlet precursor compositions.

a)

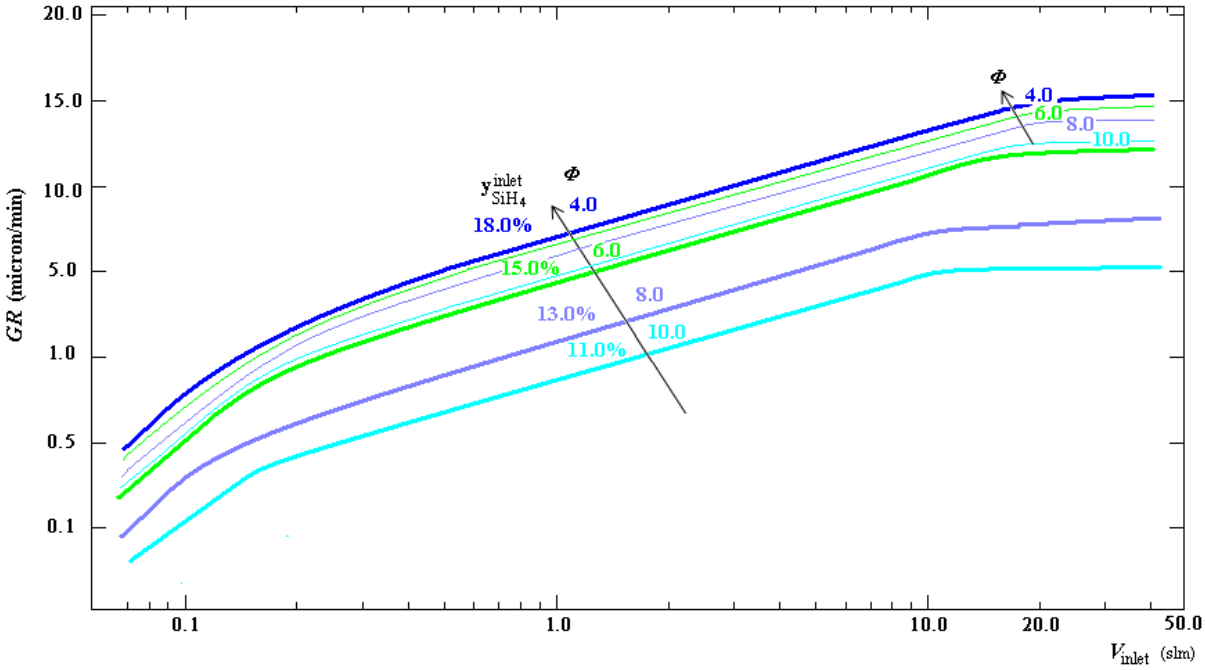

b)

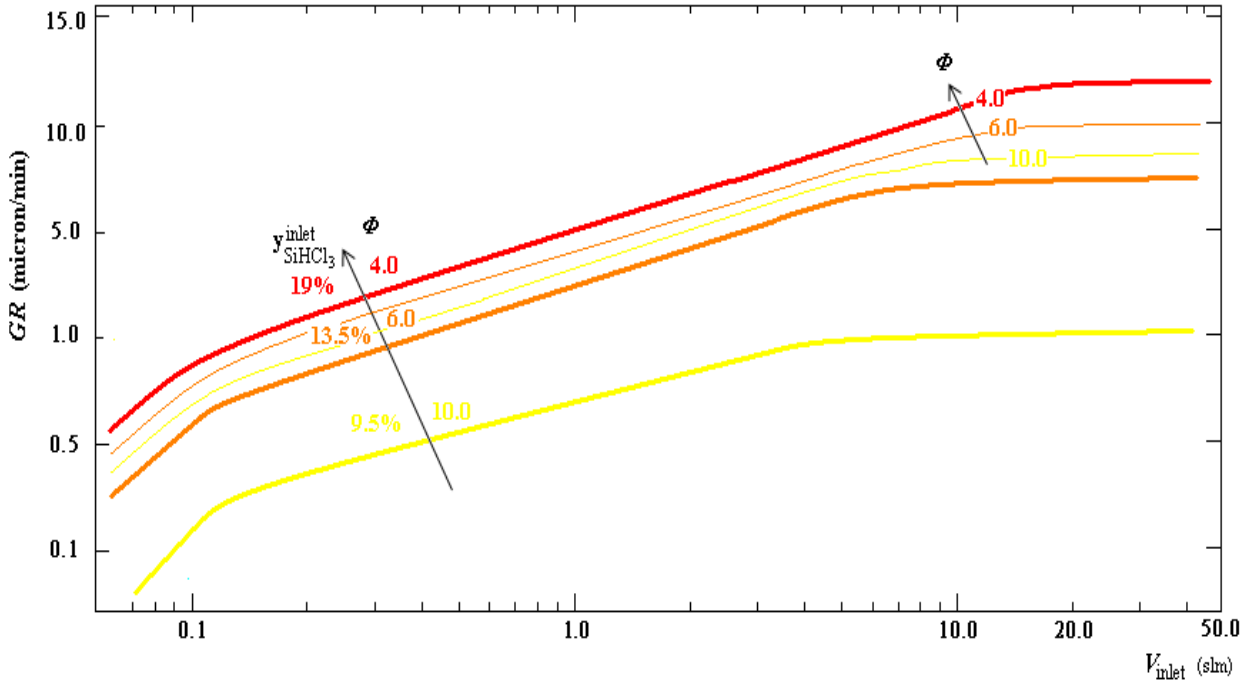

Fig. 6 – Effect of inlet flow mass rate (in terms of both inlet velocity and inlet precursors composition on the deposition rate via **a)** silane and **b)** chlorosilane routes. 0-D model results varying the oxy-fuel volumetric flow ratios (***Φ***) for fixed and variable inlet precursors compositions (thin line and thick lines respectively).

a)

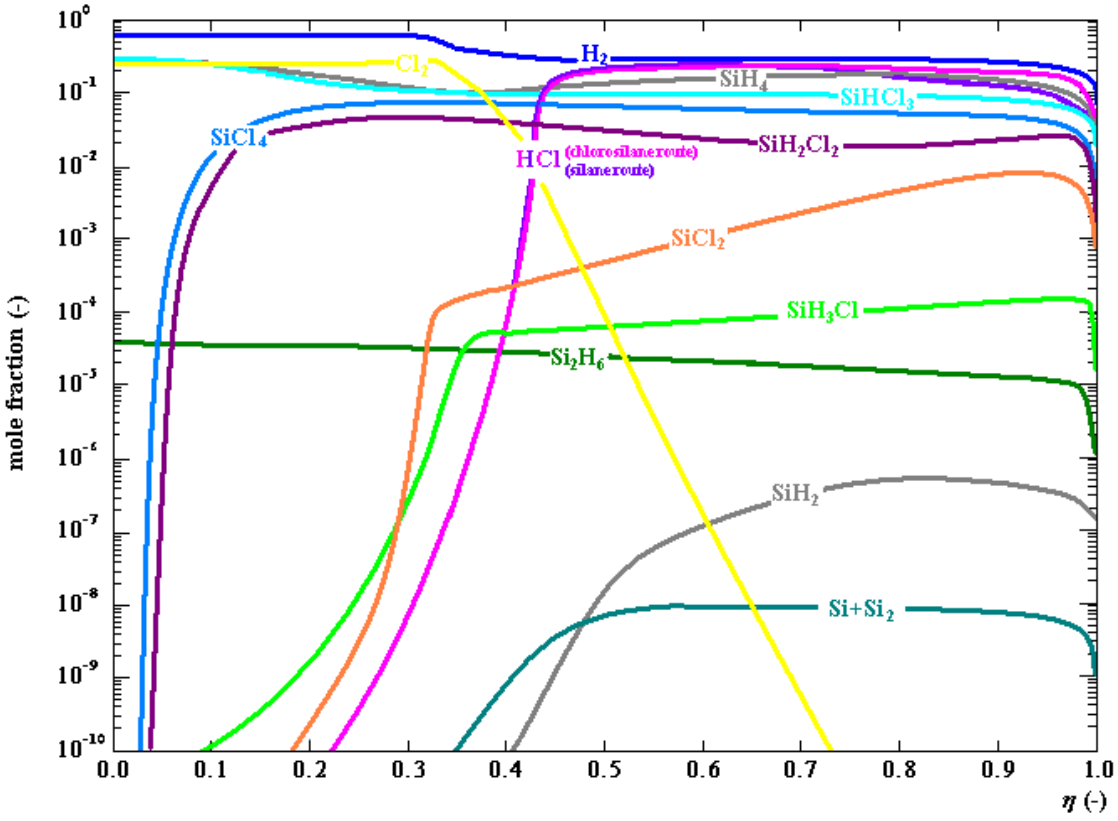

b)

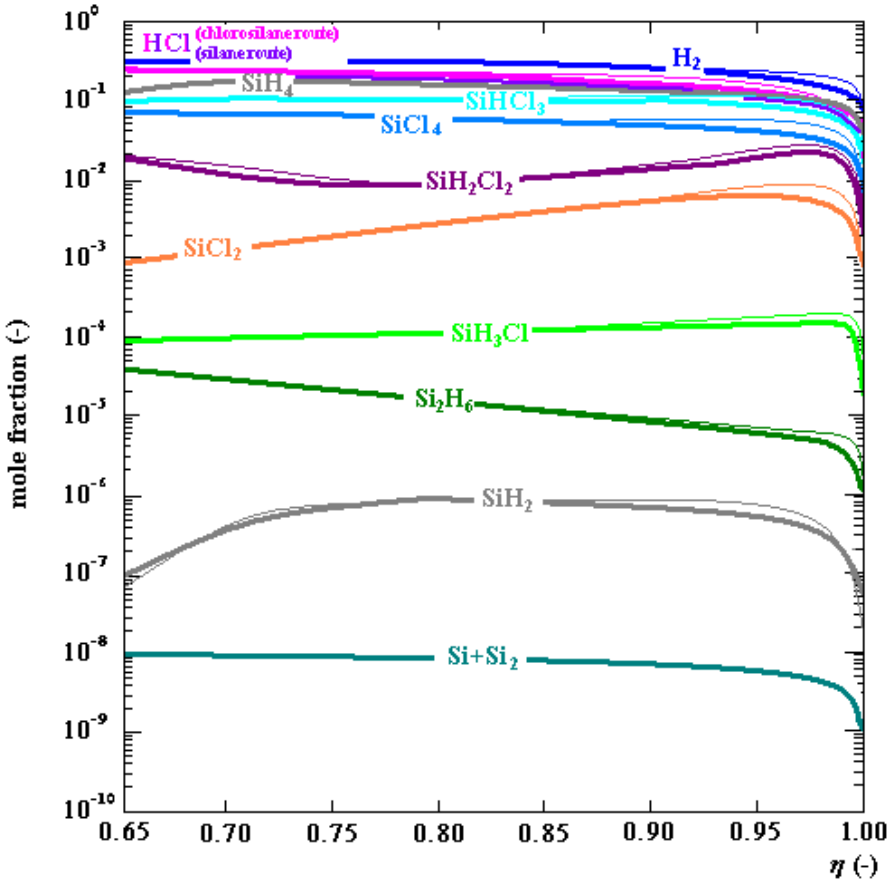

Fig. 7 – **a)** 1-D axial concentration distributions above susceptor under concentrated inlet conditions, SiH_4/H_2 and $SiHCl_3/H_2$ ≈19% vol. **b)** 1-D concentration distributions near the susceptor. Comparisons between the result from different multicomponent mass transport algorithms are shown (non-Soret Fickian approximation and SMA, thick and thin continuous lines respectively).

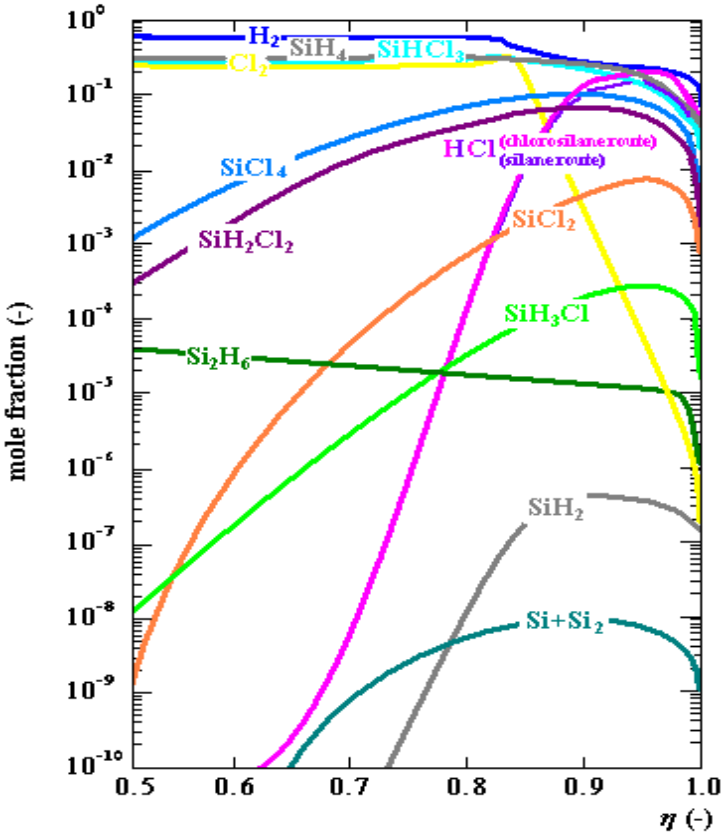

Fig. 8 – 1-D axial concentration distributions above susceptor under concentrated inlet conditions (SiH_4/H_2 and $SiHCl_3/H_2$ ≈19% vol.) for lifted flame configuration.

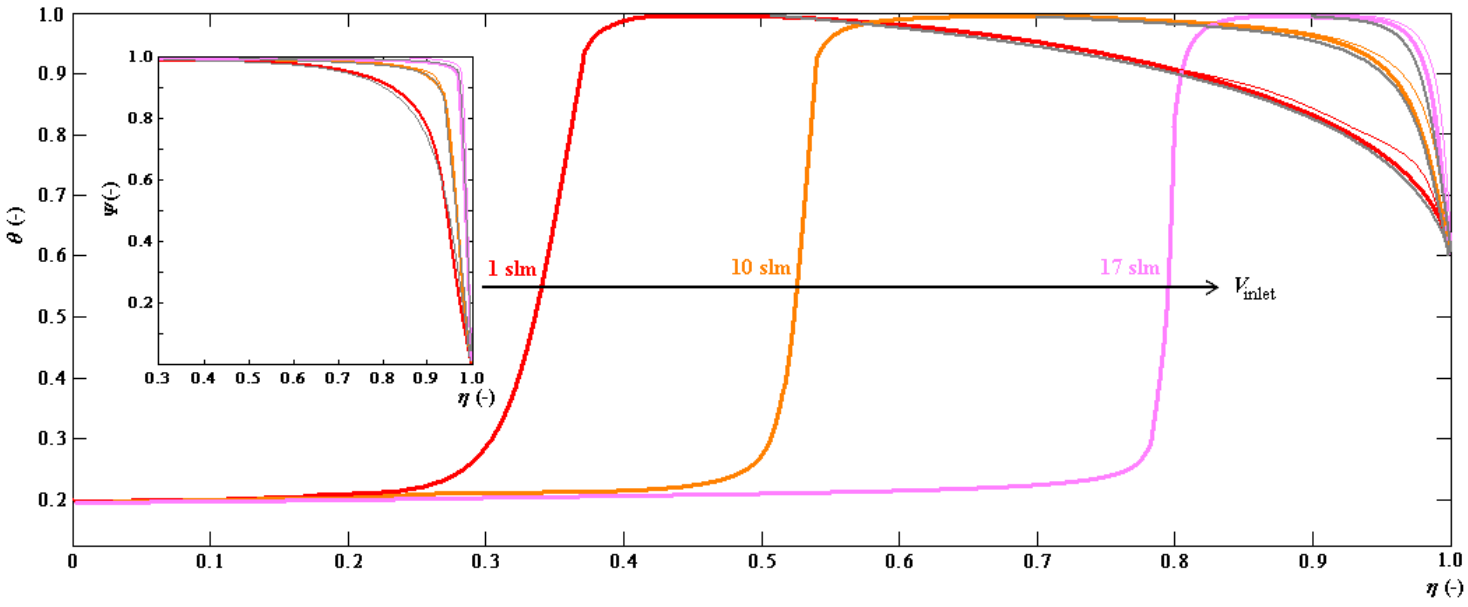

Fig. 9 – Effect of inlet flow rate on 1-D axial dimensionless temperature and velocity profiles. Comparisons between analytical, decoupled treatments and full DNS are shown (grey, thick and thin continuous lines, respectively).

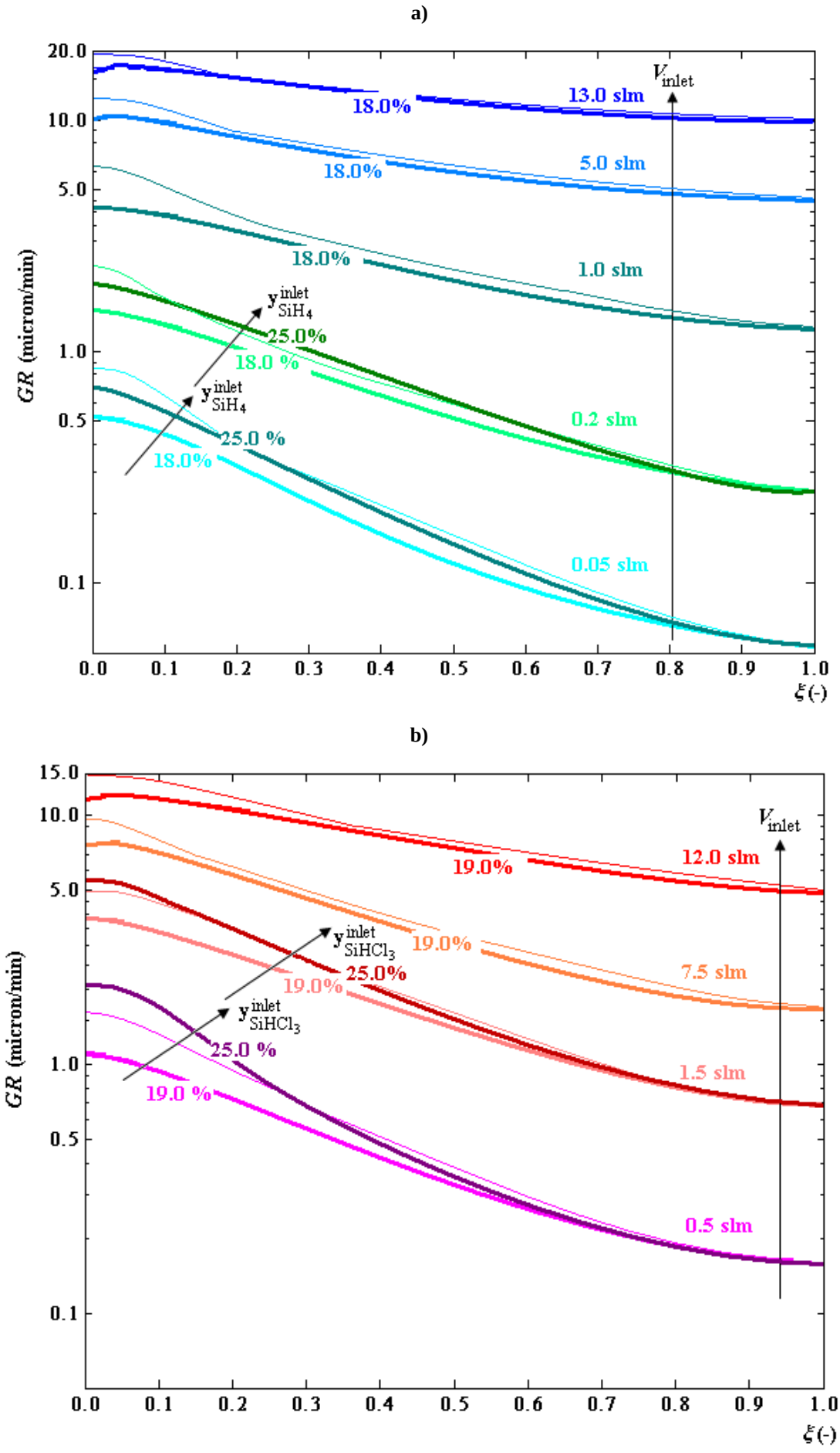

Fig. 10 – Effect of inlet flow rate and precursors composition on silicon growth via **a)** silane **b) c**hlorosilane routes. Comparisons between 2-D growth rate distributions along dimensionless radial coordinate for stagnation flow flame calculated through 2-D decoupled treatments and full 1-D DNS are shown (thick and thin lines, respectively) are shown.

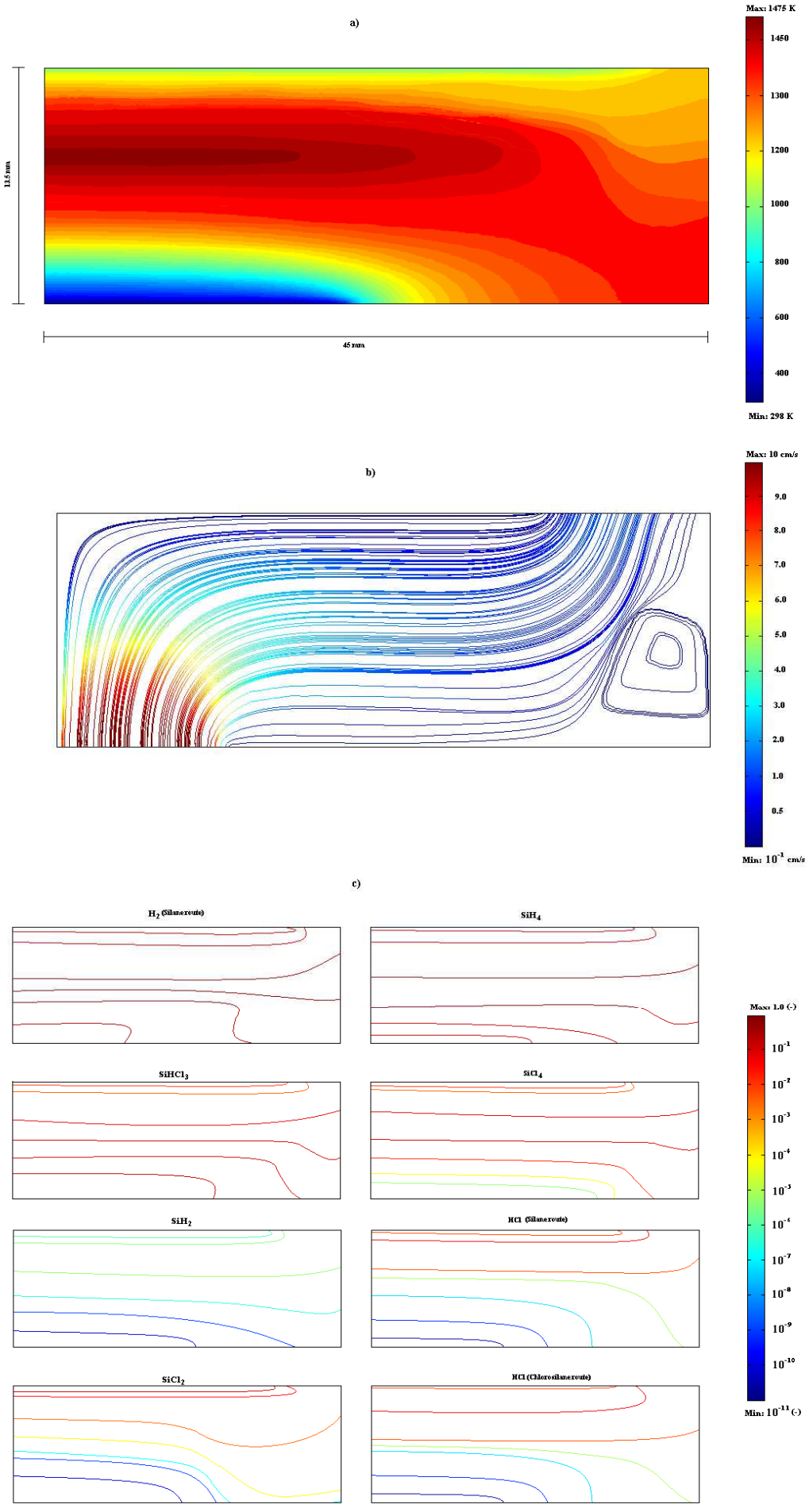

Fig. 11 – 2-D decoupled approach results for optimized stagnation flow flame deposition. **a)** temperature field (surface plot); **b)** velocity field (streamlines) and **c)** concentration field for some species (contour plots).

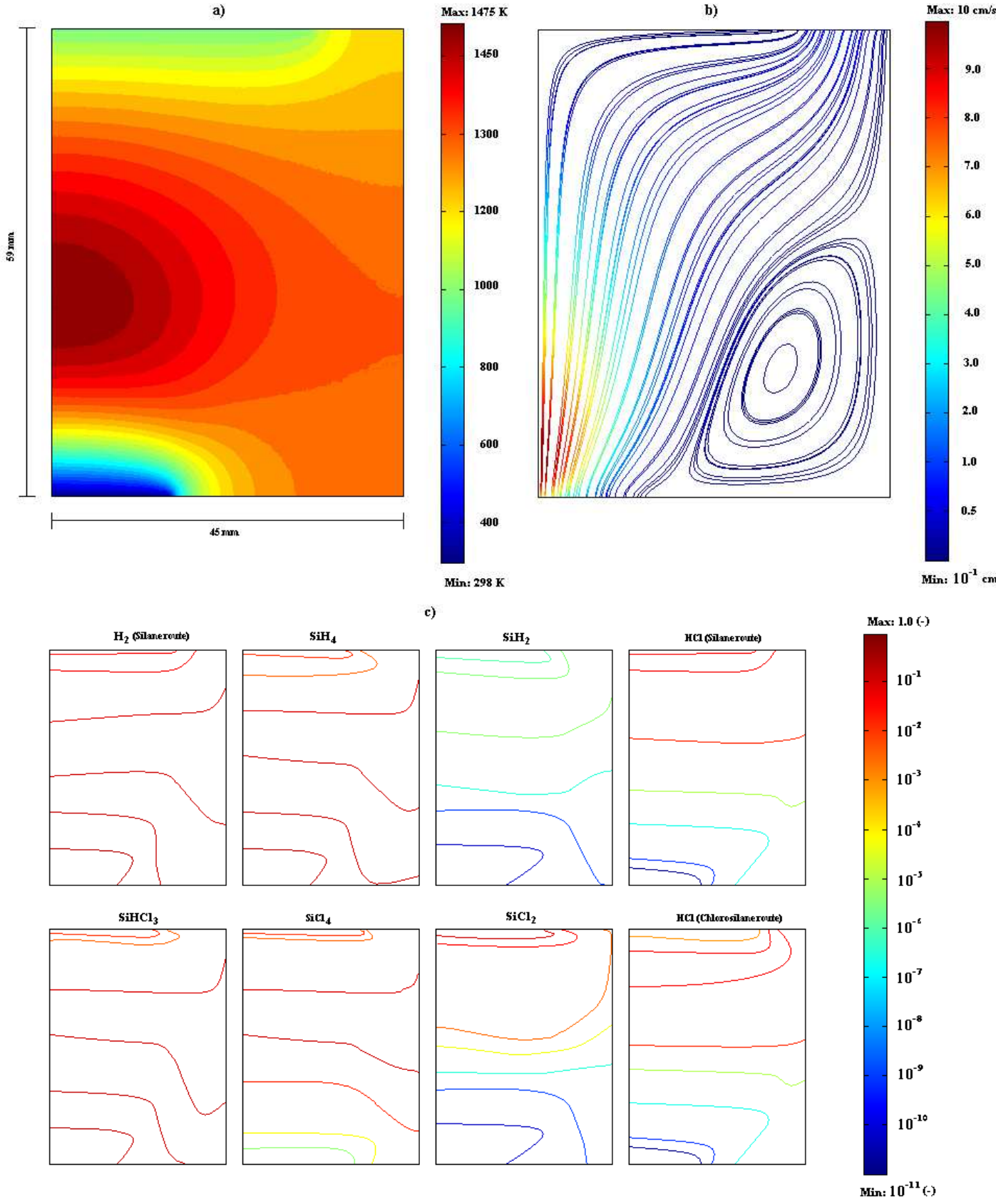

Fig. 12 – 2-D decoupled approach results for unoptimized stagnation flow flame deposition. **a)** temperature field (surface plot); **b)** velocity field (streamlines) and **c)** concentration field for some species (contour plots).

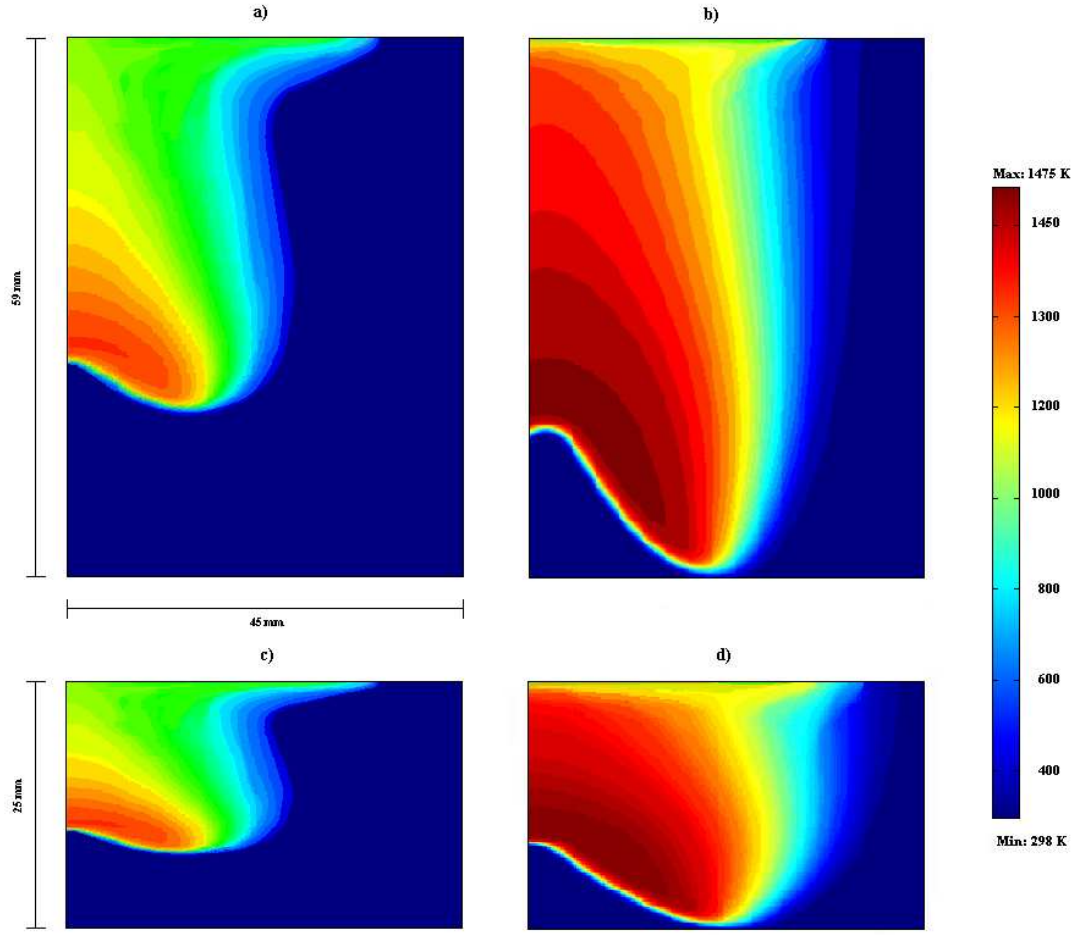

Fig. 13 –2-D temperature plots for single Bunsen flame configuration. Left and right boxes represent lifted and rim-stabilized flames, respectively.

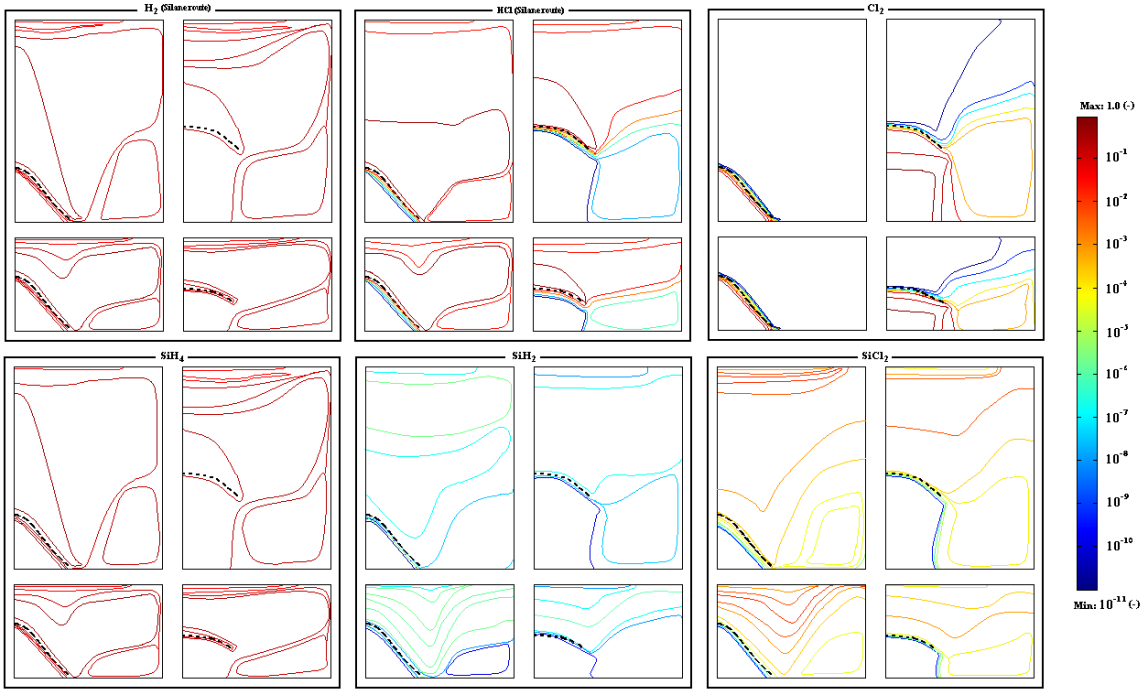

Fig. 14 – 2-D concentration contour maps of some species for single Bunsen flame configurations. For each here considered species, the two different 2-D domain are in scale. Left and right boxes represent rim-stabilized and lifted-off flames, respectively.

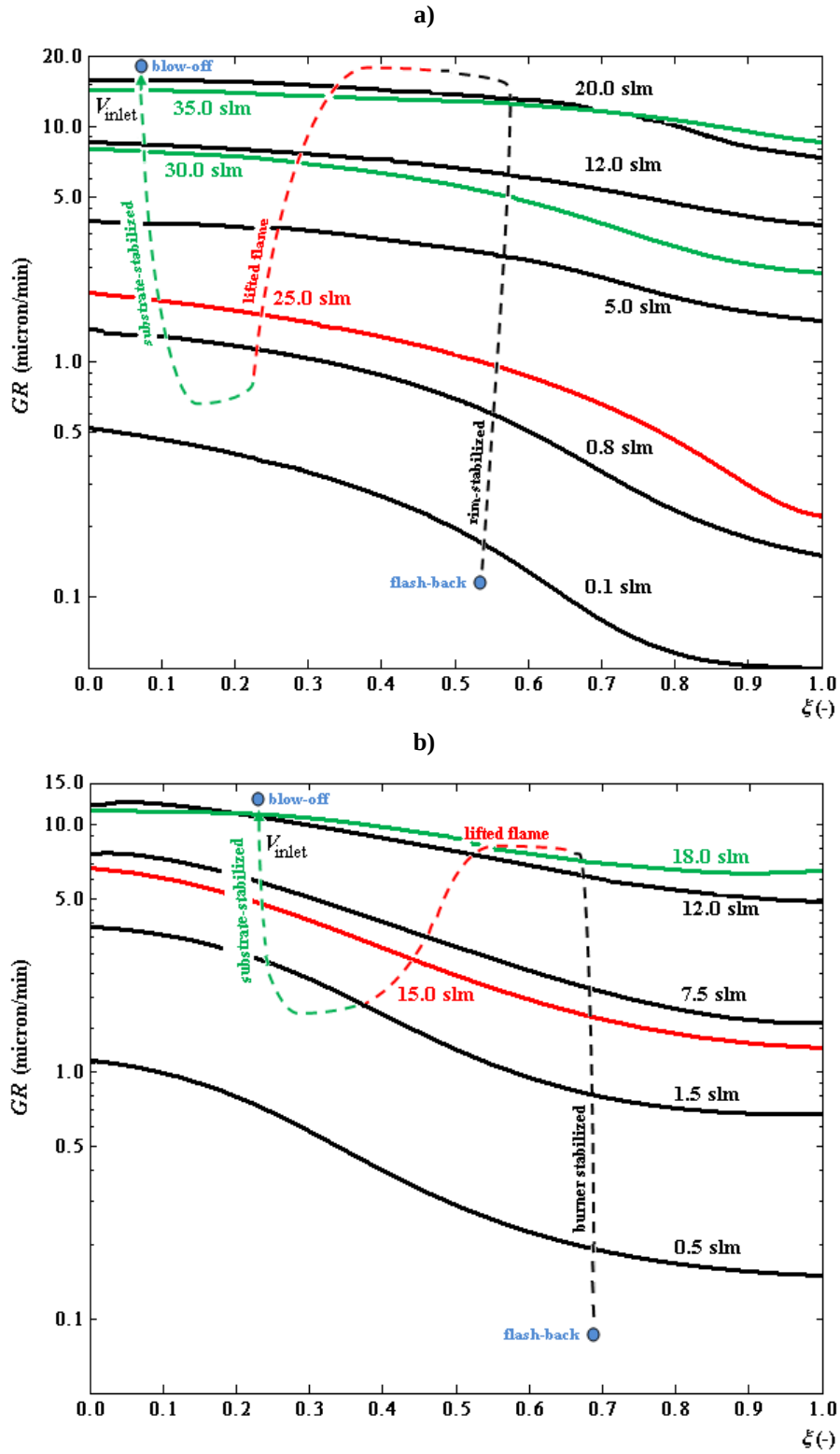

Fig. 15 – Effect of inlet flow rate on silicon growth via **a)** silane **b) c**hlorosilane routes for Bunsen flame method.

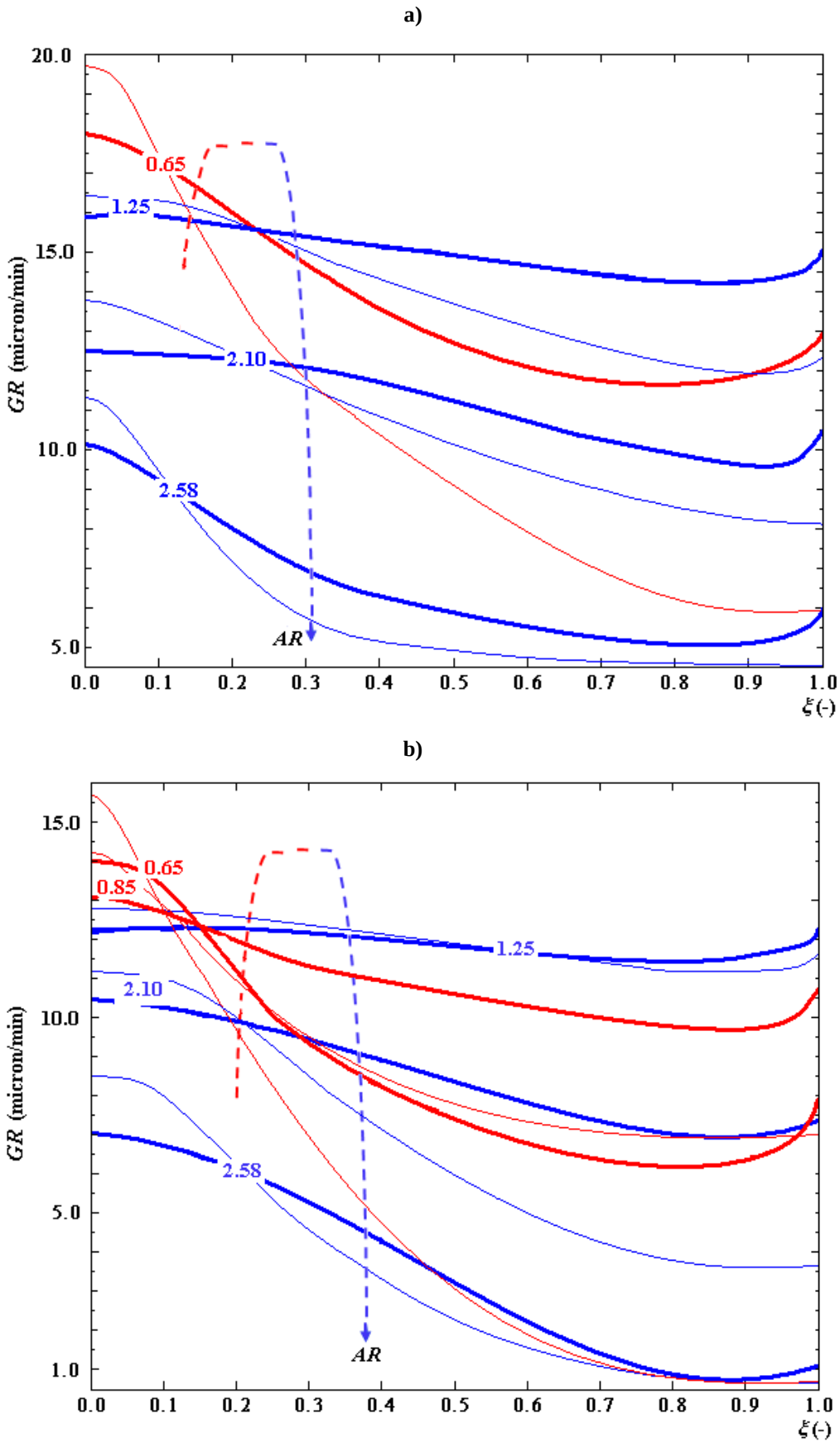

Fig. 16– Effect of standoff distance and nozzle diameter on silicon growth via **a)** silane **b) c**hlorosilane routes. Comparisons between 2-D growth rate distribution along dimensionless radial coordinate for different aspect ratio (thick and thin lines, respectively) and flame configurations (stagnation flow and Bunsen flames, blue and red lines respectively)

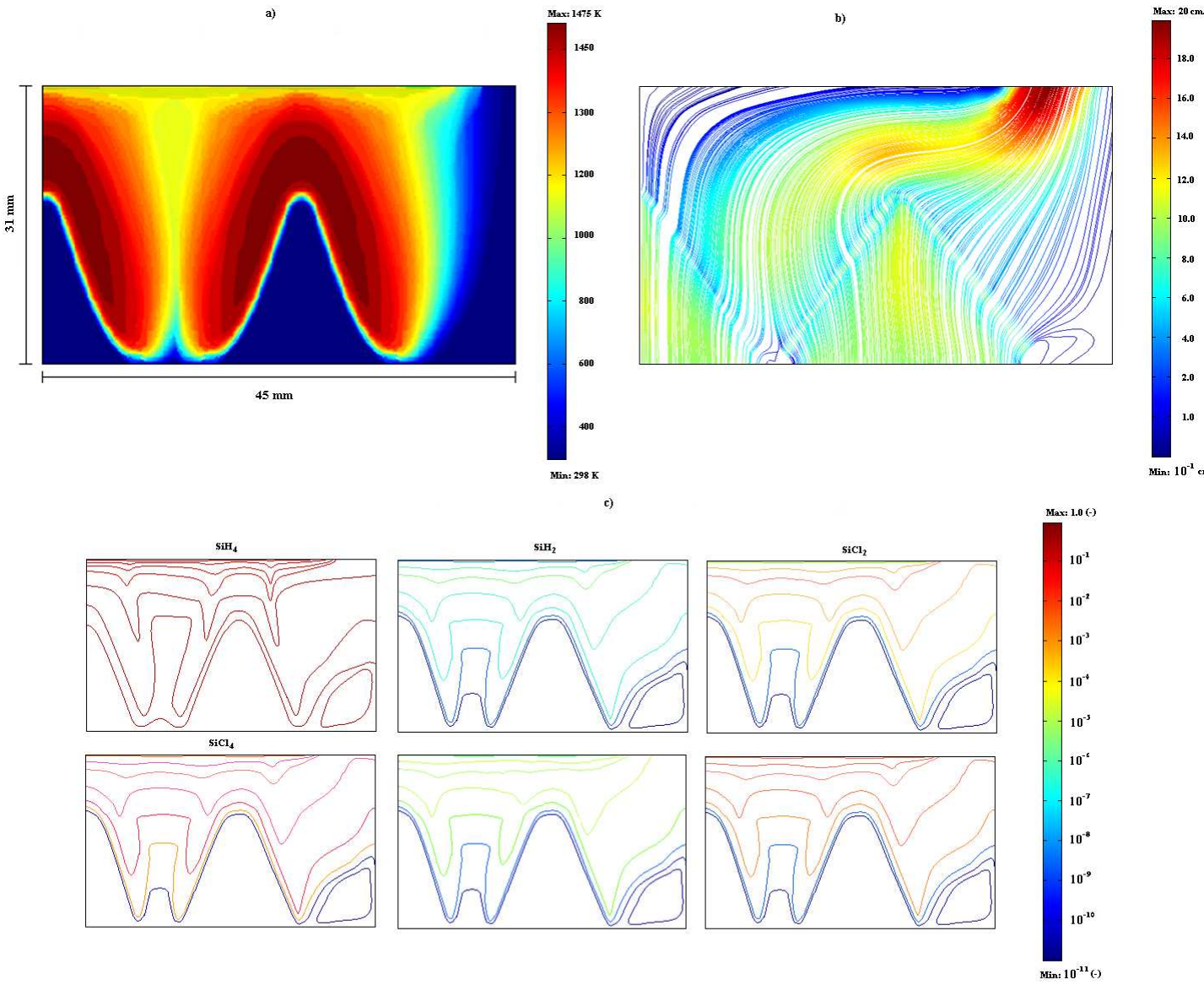

Fig. 17 – 2-D temperature plots for MNC. **a)** Temperature field (surface plot); **b)** velocity field (streamlines) and **c)** concentration field for some species (contour plots)

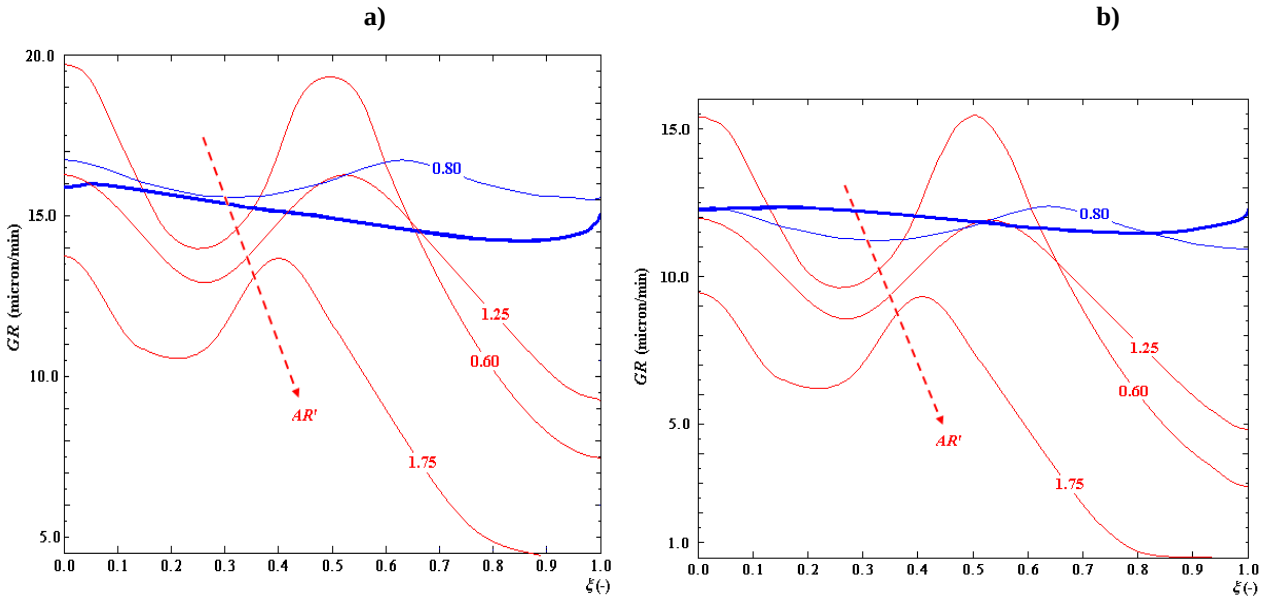

Fig. 18 – Effect of standoff distance and center-to-center separation distance on silicon growth via **a)** silane **b) c**hlorosilane routes. Comparisons between 2-D growth rate distributions along dimensionless radial coordinate for MNC for different value of the parameter *AR'* (red lines). For shake of comparison the optimum stagnation flow flame and the optimized multiple Bunsen flames configuration profiles are shown (thick and thin lines, respectively).

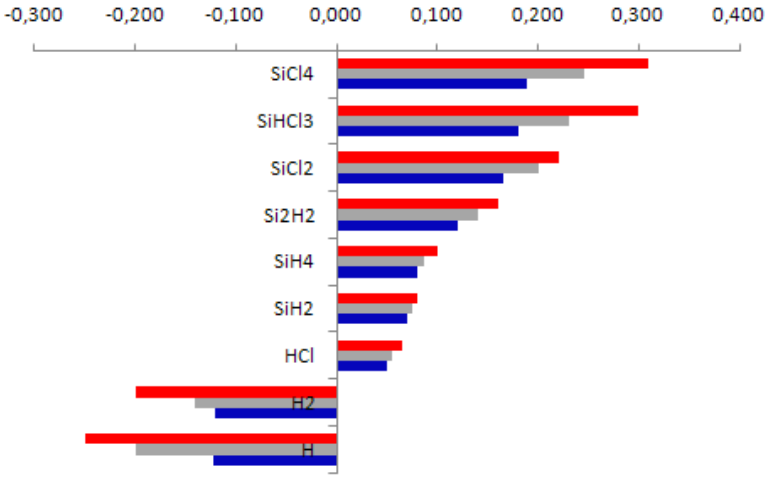

Fig. 19 – Normalized sensitivity of the species mass fluxes with respect to change in the and gas phase temperature. For shake of brevity, all species having very low sensitivity index are not reported here.

List of Tables

Table 1. a) Silane gas-phase reaction mechanisms[a]

	Reactions	log*A*	*α*	*E*	*A*	*T* ***	*T* *	*T* **
$G1_\infty$	$SiH_4 \leftrightarrow SiH_2 + H_2$	9.49	1.70	229,016				
$G1_0$		23.72	−3.54	240,904	−0.4984	888.3	209.4	2760
$G2_\infty$	$Si_2H_6 \leftrightarrow SiH_4 + SiH_2$	10.26	1.70	210,150				
$G2_0$		47.71	−10.37	234,558	-4.37×10^{-5}	438.5	2726	438.2
$G3_\infty$	$Si_2H_6 \leftrightarrow H_2 + HSiSiH_3$	9.96	1.80	226,869				
$G3_0$		38.29	−7.77	247,070	−0.1224	793.3	2400	11.39
$G4_\infty$	$Si_3H_8 \leftrightarrow SiH_2 + Si_2H_6$	12.84	1.00	220,505				
$G4_0$		63.24	−15.07	225,099	-3.5×10^{-5}	442.0	2412	128.3
$G5_\infty$	$Si_3H_8 \leftrightarrow SiH_4 + HSiSiH_3$	12.57	1.00	212,858				
$G5_0$		76.64	−17.26	248,242	0.4157	365.3	3102	9.72
$G6_\infty$	$HSiSiH_3 \leftrightarrow H_2SiSiH_2$	13.40	−0.20	22,525				
$G6_0$		27.04	−5.76	38,310	−0.4202	214.5	103	136.3
$G7_\infty$	$HSiSiH_3 + H_2 \leftrightarrow SiH_2 + SiH_4$	7.97	0.00	17,130				
$G7_0$		4.97	1.10	24,238				
$G8_\infty$	$HSiSiH_3 + SiH_4 \leftrightarrow Si_2H_6 + SiH_2$	8.24	0.40	37,250				
$G8_0$		9.42	0.10	35,468				
$G9_\infty$	$HSiSiH_3 \leftrightarrow Si + SiH_4$	13.15	0.54	240,896				
$G9_0$		36.37	−7.42	255,166	0.5336	629.2	2190	625.5
$G10_\infty$	$Si + Si_2H_6 \leftrightarrow SiH_2 + HSiSiH_3$	9.11	0.00	52,744				

[a] Kinetic parameters given in terms of mol, m, s, J, and K. Kinetic constants are expressed as $k = A\,T^{\alpha}e^{-E/RT}$. Subscripts 0, ∞, f, and b refer to low-pressure and high-pressure limits and forward and backward reactions, respectively. All values from Ho et al. (Ho, P. et al., 1994).

b) Chlorosilane gas-phase reaction mechanisms [a]

	Reactions	log*A*	*α*	*E*	*Ref.*[b]
C1	$SiHCl_3 \leftrightarrow SiCl_2 + HCl$	14.69	0.00	208.5	(Su et al., 1993)
C2	$SiH_2Cl_2 \leftrightarrow SiCl_2 + H_2$	13.92	0.00	324.0	(Su et al., 1993)
C3	$SiH_2Cl_2 \leftrightarrow HSiCl + HCl$	14.84	0.00	317.3	(Su et al., 1993)
C4	$SiCl_4 \leftrightarrow Cl + SiCl_3$	15.68	0.00	465.4	(a)
C5	$SiHCl_3 + H \leftrightarrow SiCl_3 + H_2$	6.39	0.00	10.6	(Arthur et al., 1989)
C6	$HCl \leftrightarrow H + Cl$	13.64	0.00	342.2	(Baulch et al., 1981)

[a] Kinetic parameters given in terms of mol, m, s, kJ, and K. Kinetic constants are expressed as $k = A\,T^{\alpha}e^{-E/RT}$.
[b](a) Collisional theory with sticking coefficient 0.1.

Table 2.

a)

SURFACE REACTIONS FOR SILICON GROWTH FROM SILANE AND DISILANE[a]

	Reaction	log*A*	*α*	*E*	Ref. Nos.[b]
S1	$SiH_4 + 2\sigma \rightarrow SiH_3^* + H^*$	9.06	0.5	12,600	25–29
S2	$SiH_3^* + \sigma \rightarrow SiH_2^* + H^*$	13.64	—	113,000	25–29
S3	$2SiH_2^* \rightarrow 2SiH^* + H_2$	20.38	—	188,400	25–29
S4	$Si + \sigma \rightarrow Si^*$	5.77	0.5	0	c
S5	$SiH + \sigma \rightarrow SiH^*$	5.77	0.5	0	c
S6	$Si^* \rightarrow \sigma Si_{(s)} + \sigma$	20.90	—	184,200	25–29
S7	$SiH_2 + \sigma \rightarrow SiH_2^*$	5.76	0.5	0	c
S8	$H + \sigma \rightarrow H^*$	6.63	0.5	0	c
S9	$SiH_3 + \sigma \rightarrow SiH_3^*$	5.76	0.5	0	c
S10	$Si_2H_2 + 2\sigma \rightarrow 2SiH^*$	10.56	0.5	12,600	c
S11	$SiH^* \rightarrow Si_{(s)} + \frac{1}{2}H_2 + \sigma$	11.90	—	196,700	25–29
S12	$2H^* \rightarrow H_2 + 2\sigma$	18.11	—	196,700	25–29

[a] Kinetic parameters given in terms of mol, m, s, J, and K. Rate constants are written $k = AT^{\alpha}e^{-E/RT}$. Surface reactions are written as irreversible, while rates are in mol/m^2/s.
[b] c, estimated through collisional theory [7].

b)

SURFACE REACTIONS FOR THE DEPOSITION OF SILICON FROM CHLOROSILANE'S PRECURSORS[a]

	Reaction	log A	α	E	Ref. No.(s.)[b]
G1	$SiHCl_3 \leftrightarrow SiCl_2 + HCl$	14.69	0	308.5	80
G2	$SiH_2Cl_2 \leftrightarrow SiCl_2 + H_2$	13.92	0	324.0	80
G3	$SiH_2Cl_2 \leftrightarrow HsiCl + HCl$	14.84	0	317.3	80
G4	$SiCl_4 \leftrightarrow Cl + SiCl_3$	15.68	0	465.4	(a)
G5	$SiHCl_3 + H \leftrightarrow SiCl_3 + H_2$	6.39	0	10.6	2
G6	$HCl \leftrightarrow H + Cl$	13.64	0	342.2	3
S1	$SiHCl_3 + 4\sigma \rightarrow SiCl^* + H^* + 2Cl^*$	2.05	0.5	−15.9	19, 43
S2	$SiH_2Cl_2 + 4\sigma \rightarrow SiCl^* + 2H^* + Cl^*$	2.58	0.5	−15.9	15, 43
S3	$SiCl_4 + 4\sigma \rightarrow SiCl^* + 3Cl^*$	3.84	0.5	−2.8	36, 43
S4	$H_2 + 2\sigma \rightarrow 2H^*$	5.36	0.5	72.2	7.b
S5	$HCl + 2\sigma \rightarrow H^* + Cl^*$	4.73	0.5	0	61 (a)
S6	$SiCl_2 + 2\sigma \rightarrow SiCl^* + Cl^*$	4.51	0.5	0	(b)
S7	$SiCl^* + Cl^* \rightarrow SiCl_2 + 2\sigma$	20.20	0	280.5	36
S8	$2Cl^* + Si_b \rightarrow SiCl_2 + 2\sigma$	20.20	0	280.5	36
S9	$2H^* \rightarrow H_2 + 2\sigma$	20.42	0	196.7	22
S9*	$H^* \rightarrow 1/2H_2 + \sigma$	15.30	0	238.6	22
S10	$H^* + Cl^* \rightarrow HCl + 2\sigma$	21.85	0	298.5	135
S11	$H^* + SiCl^* \rightarrow HCl + 2\sigma + Si_{(b)}$	21.85	0	298.5	61

[a] $k = AT^{\alpha}e^{-E/RT}$, expressed as s^{-1}, $m^2 \cdot mol^{-1} \cdot s^{-1}$, or $m^3 \cdot mol^{-1} \cdot s^{-1}$; T, in K; and E, in kJ/mol.

[b] (a) Collisional theory with sticking coefficient 0.1, from Ref. 61. (b) Collisional theory with sticking coefficient 0.1, assumed.

Table 3. Combustion kinetic mechanisms

a) Lumped model (Coppersthwaite D.P. et al.,1991)

Arrhenius parameters of the used H_2/Cl_2 combustion mechanism [4][a]

Reaction	k_0	E_A (kJ/mol)	ΔH (kJ/mol)
$Cl_2 + M \rightarrow 2Cl + M$	1×10^{11} m^3/(s mol)	182.9	245
$Cl + H_2 \rightarrow HCl + Cl$	1×10^{6} m^3/(s mol)	23.0	3
$H + HCl \rightarrow H_2 + Cl$	5×10^{6} m^3/(s mol)	1.7	−189
$H + Cl_2 \rightarrow HCl + Cl$	8×10^{7} m^3/(s mol)	0.6	−3
$2Cl + M \rightarrow Cl_2 + M$	1×10^{5} m^6/(s mol^2)	0	−245

[a] Rate constant: $k = k_0 \exp(E_A/RT)$, $R = 8.314$ kJ/kmol K, $[T]$ in K.

b) Detailed models (Leylegian J.C. et al., 2005)

Table 1
Kinetic mechanism for $H_2 + Cl_2$ reaction system

No.	Reaction[a]	A	n	E	Ref.
1	$Cl_2 + M = Cl + Cl + M$	5.74E+15	0	55,596	[a]
2	$Cl + H_2 = HCl + H$	2.88E+08	1.58	3,199	[37]
3	$H + Cl_2 = HCl + Cl$	9.64E+13	0	1,680	[34]
4	$H + H + M = H_2 + M$	6.53E+17	−1	0	[52][b]
5	$H + H + N_2 = H_2 + N_2$	5.43E+18	−1.3	0	[53]
6	$H + H + H_2 = H_2 + H_2$	9.79E+16	−0.6	0	[52]
7	$HCl + M = H + Cl + M$	4.40E+13	0	81,753	[22]
8	$H + Cl_2 = HCl + Cl$	9.64E+08	0	1,680	[a]
9	$H + Cl_2 = HCl(v = 1) + Cl$	2.31E+11	0	1,680	[a]
10	$H + Cl_2 = HCl(v = 2) + Cl$	8.38E+12	0	1,680	[a]
11	$H + Cl_2 = HCl(v = 3) + Cl$	5.27E+13	0	1,680	[a]
12	$H + Cl_2 = HCl(v = 4) + Cl$	3.51E+13	0	1,680	[a]
13	$H + Cl_2 = HCl(v = 5) + Cl$	2.51E+10	0	1,680	[a]
14	$Cl + H_2 = HCl(v = 1) + H$	2.88E+08	1.58	11,408	[a]
15	$Cl + H_2 = HCl(v = 2) + H$	2.88E+08	1.58	19,283	[a]
16	$Cl + H_2 = HCl(v = 3) + H$	2.88E+08	1.58	26,837	[a]
17	$Cl + H_2 = HCl(v = 4) + H$	2.88E+08	1.58	34,025	[a]
18	$Cl + H_2 = HCl(v = 5) + H$	2.88E+08	1.58	40,869	[a]
19	$Cl + H_2 = HCl(v = 6) + H$	2.88E+08	1.58	47,372	[a]
20	$HCl(v = 1) + M = HCl + M$	8.00E+01	3.0	0	[27]
21	$HCl(v = 2) + M = HCl(v = 1) + M$	1.60E+02	3.0	0	[27]
22	$HCl(v = 3) + M = HCl(v = 2) + M$	2.40E+02	3.0	0	[27]
23	$HCl(v = 4) + M = HCl(v = 3) + M$	3.20E+02	3.0	0	[27]
24	$HCl(v = 5) + M = HCl(v = 4) + M$	4.00E+02	3.0	0	[a]
25	$HCl(v = 6) + M = HCl(v = 5) + M$	4.80E+02	3.0	0	[a]
26	$HCl(v = 1) + HCl(v = 5) = HCl + HCl(v = 6)$	2.30E+12	0.5	7,600	[a]
27	$HCl(v = 1) + HCl(v = 4) = HCl + HCl(v = 5)$	2.30E+12	0.5	7,600	[27]
28	$HCl(v = 1) + HCl(v = 3) = HCl + HCl(v = 4)$	2.30E+12	0.5	7,600	[27]
29	$HCl(v = 1) + HCl(v = 2) = HCl + HCl(v = 3)$	2.10E+13	0.5	6,000	[27]
30	$HCl(v = 1) + HCl(v = 1) = HCl + HCl(v = 2)$	7.00E+12	0.5	2,400	[27]
31	$HCl(v = 2) + HCl(v = 5) = HCl(v = 1) + HCl(v = 6)$	2.30E+12	0.5	7,600	[a]
32	$HCl(v = 2) + HCl(v = 4) = HCl(v = 1) + HCl(v = 5)$	2.30E+12	0.5	7,600	[27]
33	$HCl(v = 2) + HCl(v = 3) = HCl(v = 1) + HCl(v = 4)$	2.10E+13	0.5	6,000	[27]
34	$HCl(v = 2) + HCl(v = 2) = HCl(v = 1) + HCl(v = 3)$	7.00E+12	0.5	2,400	[27]
35	$HCl(v = 3) + HCl(v = 5) = HCl(v = 2) + HCl(v = 6)$	2.10E+13	0.5	6,000	[a]
36	$HCl(v = 3) + HCl(v = 4) = HCl(v = 2) + HCl(v = 5)$	2.10E+13	0.5	6,000	[27]
37	$HCl(v = 3) + HCl(v = 3) = HCl(v = 2) + HCl(v = 4)$	7.00E+12	0.5	2,400	[27]
38	$HCl(v = 1) + Cl_2 = HCl + Cl + Cl$	2.00E+13	0	46,610	[a]
39	$HCl(v = 2) + Cl_2 = HCl + Cl + Cl$	2.00E+13	0	38,735	[a]
40	$HCl(v = 3) + Cl_2 = HCl + Cl + Cl$	2.00E+13	0	31,202	[a]
41	$HCl(v = 4) + Cl_2 = HCl + Cl + Cl$	2.00E+13	0	24,014	[a]
42	$HCl(v = 5) + Cl_2 = HCl + Cl + Cl$	2.00E+13	0	17,170	[a]
43	$HCl(v = 6) + Cl_2 = HCl + Cl + Cl$	2.00E+13	0	10,667	[a]

[a] This work, see text.
[b] The third body collision enhancement factor for **H** atom is taken as 20.

Table 4. a) 0-D **s**urface concentration for the main important species.
dilute ($SiHCl_3/H_2 \approx 2\%$ vol.) vs. concentrated ($SiHCl_3/H_2 \approx 15\%$ vol.) feed stream
lumped vs. detailed surface kinetic schemes
equilibrium vs reacting flow

Species	Dilute feed streams				Concentrated feed stream			
	Thermodynamics Equil.		Reacting Gas Flow		Thermodynamics Equil.		Reacting Gas Flow	
	Lumped	Detailaed	Lumped	Detailaed	Lumped	Detailaed	Lumped	Detailaed
H_2	0.11510	0.11337	0.09120	0.08233	0.11520	0.11345	0.10320	0.08233
HCl	0.09460	0.10519	0.08234	0.07519	0.00916	0.10514	0.09530	0.07519
$SiHCl_3$	0.00834	0.00945	0.00634	0.00715	0.00844	0.00943	0.00954	0.00715
SiH_3Cl	0.00010	0.00040	0.00223	0.00345	0.00234	0.00533	0.00301	0.00345
$SiCl_2$	0.00524	0.00278	0.00124	0.00134	0.00522	0.00275	0.00180	0.00134

b) 1-D **s**urface concentration for the main important species.
dilute ($SiHCl_3/H_2 \approx 2\%$ vol.) vs. concentrated ($SiHCl_3/H_2 \approx 15\%$ vol.) feed stream
lumped vs. detailed surface kinetic schemes
equilibrium vs reacting flow

Species	Dilute feed streams				Concentrated feed stream			
	Thermodynamics Equil.		Reacting Gas Flow		Thermodynamics Equil.		Reacting Gas Flow	
	Lumped	Detailaed	Lumped	Detailaed	Lumped	Detailaed	Lumped	Detailaed
H_2	0.09510	0.11005	0.08200	0.08450	0.09120	0.09341	0.08320	0.08388
HCl	0.08460	0.00899	0.07834	0.07944	0.00716	0.06140	0.05530	0.06519
$SiHCl_3$	0.00737	0.00781	0.00542	0.00342	0.00446	0.00457	0.00954	0.00413
SiH_3Cl	0.00003	0.00000	0.00212	0.00226	0.00131	0.00555	0.00301	0.00645
$SiCl_2$	0.00421	0.00406	0.00043	0.00009	0.00232	0.00156	0.00180	0.00134

Table 5. Comparisons between 0-D and 1-D species concentration distributions at wafer surface for chemically reacting concentrated feed stream, $SiHCl_3/H_2 \approx 15\%$ vol.

- **a)** Wilke-simplified non-Soret Fickian model (0-D)
- **b)** Soret-Fickian model (1-D)
- **c)** full multicomponent transport models (1-D)
- **d)** Soret full multicomponent transport models (1-D)

Species	**a)**	**b)**	**c)**	**d)**
H_2	0.08388	0.06778	0.07350	0.08781
HCl	0.05569	0.0469	0.05099	0.0469
$SiHCl_3$	0.00373	0.00573	0.00436	0.00552
$SiCl_4$	0.00356	0.00456	0.00369	0.00479
SiH_3Cl	0.00235	0.00335	0.00278	0.00325
$SiCl_2$	0.00134	0.00234	0.00184	0.00214
SiH_2Cl_2	0.00218	0.00418	0.00218	0.00318

References

IEA International Energy Agency, Key World Energy Statistics, 2007, www.iea.org.

Smalley R. E., 2005. Future Global Energy Prosperity: The Terawatt Challenge, MRS Bulletin 30, 412.

Rogol M., 2004. Solar Power through 2020: Potential and Challenges, presented at the MIT Laboratory for Energy and the Environment's Environment and Sustainability Seminar Series,. http://esd.mit.edu/esd_reports/summer2005/solar_power.html

Masi, M., Carra, S., Vaccari, G., Crippa, D., 1997. Optimization of SiO2 atmospheric deposition in continuous belt systems. Electrochemical Society Proceedings 97 (25), 1167–1174.

Nieto J.P., Jeannero L., Caussat B., 2005. Modelling of an industrial moving belt chemical vapour deposition reactor forming SiO2 films, Chemical Engineering Science 60, 5331–5340.

Wilson K. S. Chiu, Yogesh Jaluria, Continuous chemical vapor deposition processing with a moving finite thickness susceptor, J. Mater. Res. 15 (2) 2000 317-328. **DOI:** 10.1557/JMR.2000.0050.

Tzeng Y., Phillips R., Cutshaw C., Srivinyunon T., Loo B. H. and Wang P., 1991. Multiple flame deposition of diamond films, Appt. Phys. Lett. 58 (23), 2645–2647.

Tzeng Y., Kung P. J., Zee R., Legg K., Legg H. S., Burns D., and Loo B. H., 1988. Appl. Phys. Lett. 53, 2326-2335.

Yarbrough W.A., Stewart M.A, Cooper J.A. Jr, 1989. Combustion synthesis of diamond, Surface and Coatings Technology, 39 (40), 241-252.

Hirose Y. and Kondo N., Program and Book of Abstracts, 35th Japan Society of Applied Physics Spring Meeting (Japan Society of Applied Physics, Tokyo, 1988), p. 434.

Masi M., Fiorucci A., Camarda M., Antonino La Magna, Francesco La Via, 2009. Multiscale Simulation for Epitaxial Silicon Carbide Growth by Chlorides Route, Thin Solid Films. doi: 10.1016/j.tsf.2009.10.045.

Barbato A., Fiorucci A., Rondanini M., Cavallotti C., 2007. Multiscale investigation of the influence of surface morphology on thin film CVD, Surface & Coatings Technology 201, 8884–8887.

Bloem J., 1980, J. Crystal Growth, 50, 581.

Gilmer G. H. and Broughton J. Q., 1986. Ann. Rev. Mater. Sci., 16, 487.

J. A. Venables, G. D. T. Spiller and M. Hanbrucka, Rep. Progr. Phys., 1984, 47, 399.

A. Madhukar and S. A. Chaisas, in CRC Crit. Rev. Soild State Mater. Sci., 1988, 14, 1.

N.G. Glumac and D.G. Goodwin, Large-area diamond film growth in a low-pressure flame Materials Letters 18 (1993) 1l9- 122 North-Holland

D. G. Goodwin, Scaling laws for diamond chemical-vapor deposition. I. Diamond surface chemistry,J. Appl. Phys. 74 (1 I), 1 December 1993

Murayama M., Kojima, S., and Uchida, K., J. Appl. Phys. 69:7924-7926 (1991)
M. Okkerse, C. R. Kleijn, and H. E. A. van den Akker, Two-dimensional simulation of an oxy-acetylene torch diamond reactor with a detailed gas-phase and surface mechanism, JOURNAL OF APPLIED PHYSICS VOLUME 88, number 71 (2000)

Masi M., Di Stanislao M., Veneroni A., 2003. Fluid-dynamics during vapor epitaxy and modeling, Progress in Crystal Growth and Characterization of Materials 47, 239-270.

Masi M., Komu S., Epitaxial Growth Modeling, in Semiconductiors and Materials., vol.72 (2001) 185-224

Ellen Meeks, Harry K. Moffat, Joseph F. Grcar, and Robert J. Kee , SAND96-8218 • UC–405 AURORA: A FORTRAN Program for Modeling Well Stirred Plasma and Thermal Reactors with Gas and Surface Reactions, 1996

Cavalloti C. and Masi M., Epitaxial Growth Theory: Vapor-Phase and Surface Chemistry, in Semiconductiors and Materials., vol.72 (2001) 51-88

Masi M., Fogliani S., Carrà S., Modeling and optimization of barrel ractors for epitaxial silicon CVD, in Chemical Vapor Deposition XIII. Eds. T. M. Besmann, M. D. Allendorf, McD. Robinson, and R. K. Ulrich, The Electrochemical Society, Pennington NJ, 125 (1996).

Masi M., Multiscale approach to material synthesis by gas phase deposition, Journal de Physique IV 11 (2001) 117-128

MOTOHIDE MURAYAMA* and KIYOSHI UCHIDA, COMBUSTION AND FLAME 91:239-245 (1992) 239 Synthesis of Uniform Diamond Films by Flat Flame Combustion of Acetylene / Hydrogen / Oxygen Mixtures

Varma A., Morbidelli M., Wu H., Parametric sensitivity in chimical systems, 1999

Dandy S.D. and Coltrin M.E., A simplified analytical model of diamond growth in direct current arcjet reactors, J. Mat. Res. Vol 10, num. 8, 1995

C.A. Wang, S. Patnaik, J.W. Caunt, R.A. Brown, Growth characteristics of a vertical rotating-disk OMVPE reactor, J. Cryst. Growth 93 (1988) 228–234.

W.K. Cho, D.H. Choi, M.-U. Kim, Optimization of the inlet concentration profile for uniform deposition in a cylindrical chemical vapor deposition chamber, Int. J. Heat Mass Transfer 42 (1999) 1141–1146.

W.K. Cho, D.H. Choi, M.-U. Kim, Optimization of the inlet velocity profile for uniform epitaxial growth in a vertical metalorganic chemical vapor deposition reactor, Int. J. Heat Mass Transfer 42 (1999) 4143–4152
5500 Series Atmospheric Pressure CVD Systems, retrieved 30 December 2003 from http://www.sierratherm.com/prod5500.htm.

Schlicting, H., Boundary Layer Theory. 6th Ed., New York: McGraw-Hill (1968)

G. Luo, S.P. Vanka , N. Glumac, Fluid flow and transport processes in a large area atmospheric pressure stagnation flow CVD reactor for deposition of thin films, International Journal of Heat and Mass Transfer 47 (2004) 4979–4994

S.P. Vanka, G. Luo, N.G. Glumac, Parametric effects on thin film growth and uniformity in an atmospheric pressure impinging jet CVD reactor, J. Cryst. Growth 267 (1–2) (2004) 22–34.

S.P. Vanka, G. Luo, N.G. Glumac, Numerical study of mixed convection flow in an impinging jet CVD reactor for atmospheric pressure deposition of thin films, ASME J. Heat Transfer (2004), in press.
Y. WANG, C. CHAUSSAVOINE and F. TEYSSANDIER, JOURNAL DE PHYSIQUE IV Colloque C2, suppl. au Journal de Physique 11, Vol 1, septembre 1991 2D MODELLING OF SILICON HEMICAL VAPOR DEPOSITION IN AN IMPINGING JET REACTOR

D.I. Fotiadis, A.M. Kremer, D.R. McKenna, K.F. Jensen, Complex flow phenomena in vertical MOVCD reactors: effects on deposition uniformity and interface abruptness, J. Cryst. Growth 85 (1987) 154–164.

D.I. Fortiadis, S. Kieda, K.F. Jensen, Transport phenomena in vertical reactors for metalorganic vapor phase epitaxy, Journal of Crystal Growth 102 (1990) 441-470

S. Patnaik, R.A. Brown, C.A. Wang, Hydrodynamic dispersion in rotating-disk OMVPE reactors: numerical simulation and experimental measurements, Journal of Crystal Growth 96 (1989) 153-174

Stewart G.D., MS Thesis, 1995

Dollet A. et al., Surface and Coatings Technology 177 –178 (2004) 382–388
A.N. Vorob'ev, S.Yu. Karpov, M.V. Bogdanov, A.E. Komissarov, O.V. Bord, A.I. Zhmakin, Yu.N.

Makarov, Numerical study of SiC CVD in a vertical cold-wall reactor, Computational Materials Science 24(2002) 520–534

G. Evans, R. Greif, A Numerical Model of the Flow and Heat Transfer in a Rotating Disk Chemical Vapor Deposition Reactor, J. Heat Transfer 109 (1987) 928–935

Evans, G.H. and Greif, R., "Effects of Boundary Conditions on the Flow and Heat Transfer in a Rotating Disk Chemical Vapor Deposition Reactor," Num. Heat Trans., 12, 243-252 (1987)

Breiland, W.G. and Evans, G.H., "Design and Verification of Nearly Ideal Flow and Heat Transfer in a Rotating Disk Chemical Vapor Deposition Reactor," J. Electrochem. Soc., 138(6), 1806-1816 (1991)

S. Joh, G. H. Evans, Heat Transfer and Flow Stability in a Rotating Disk/Stagnation Flow Chemical Vapor Deposition Reactor, SANDIA REPORT SAND96-8253 l UC-1409 (1996)

S. Joh, G. H. Evans, HEAT TRANSFER AND FLOW STABILITY IN A ROTATING DISK STAGNATION FLOW CHEMICAL VAPOR DEPOSITION REACTOR, Numerical Heat Transfer, Part A: Applications, 31: 8, 867 — 879 (1997)

W. S. Winters, G. H. Evans, R. Greif, The Influence of Convective Heat Transfer on Flow Stability in Rotating Disk Chemical Deposition Reactors, SANDIA REPORT, SAND97–8266 l UC-401 (June 1997)

W. S. WINTERS and G. H. EVANS, Mixed binary convection in a rotating disk chemical vapor deposition reactor, Int. J. Heat Mass Transfer. Vol. 40, No. 3, pp. 737-744, 1997, TECHNICAL NOTES

M.E. Coltrin, R.J. Kee, G.H. Evans, J. Electrochem. Soc. 136 (3) (1989) 819.

M. E. Coltrin, R. J. Kee, and J. A. Miller, A Mathematical Model of Silicon Chemical Vapor Deposition, J. Electrochem. Soc., vol. 133, pp. 1206–1213, 1986.

C. Houtman, D. B. Graves, and K. F. Jensen, CVD in Stagnation Point Flow, J. Electrochem. – An Evaluation of the Classical 1D Treatment Soc., vol. 133, pp. 961–969, 1986

C. R. Kleijn and C. J. Hoogendoorn, A Study of 2- and 3-D Transport Phenomena in Horizontal Chemical Vapor Deposition Reactors, Chem. Eng. Sci., vol. 46, pp. 321–334, 1991.

C.R. Kleijn, Computational modeling of transport phenomena and detailed chemistry in chemical vapor deposition - a benchmark solution, Thin Solid Films 365 (2000) 294-306

K.J. Kuijlaars, C.R. Kleijn, H.E.A. van den Akker, Modeling of selective tungsten low-pressure chemical vapor deposition, Thin Solid Films 290-291 (1996) 406-410

S. A. Gokoglu, Chemical Vapor Deposition Modeling—An Assessment of Current Status, in K. E. Spear and G. W. Cullen (eds.), Proc. Eleventh Int. Conf. on Chemical Vapor Deposition, Seattle, WA, October 1990, pp. 1–9.

R. L. Mahajan and C. Wei, Buoyancy, Soret, Dufour, and Variable Property Effects in Silicon Epitaxy, J. Heat Transfer, vol. 113, pp. 688–695, 1991.

G. W. Young, S. I. Hariharan, R. Carnahan, Flow Effects in a Vertical CVD Reactor, SIAM Journal on Applied Mathematics, Vol. 52, No. 6 (Dec., 1992), pp. 1509-1532

M. PONS, R. KLEIN, C. ARENA and S. MARIAUX, MODELING OF COLD WALL CHEMICAL VAPOR DEPOSITION REACTORS (FOR SEMICONDUCTOR FABRICATION), JOURNAL DE PHYSIQUE, Colloque C5, supplement au n°5, Tome 50, may 1989, http://dx.doi.org/10.1051/jphyscol:1989510

W.K. Cho, D.H. Choi, M. Kim, Optimization of inlet concentration profile for uniform deposition in a cylindrical chemical vapor deposition chamber, Technical Note, International Journal of Heat and Mass Transfer 42 (1999) 1141-1146

W.K. Cho, D.H. Choi, M.-U. Kim, Optimization of the inlet velocity profile for uniform epitaxial growth in a vertical metalorganic chemical vapor deposition reactor, International Journal of Heat and Mass Transfer 42 (1999) 4143-4152

C. L. Leakeas, M. A. R. Sharif, EFFECTS OF THERMAL DIFFUSION AND SUBSTRATE TEMPERATURE ON SILICON DEPOSITION IN AN IMPINGING-JET CVD REACTOR, Numerical Heat Transfer, Part A: Applications, 44: 2, 127 — 147 (2003)

C. Theodoropoulos et al., Journal of Crystal Growth 217 (2000) 65-81

G. Mihopoulos, Steven G. Hummel, Klavs F. Jensen, Simulation of flow and growth phenomena in a close-spaced reactor, Journal of Crystal Growth 195 (1998) 725-732
AP CVD modeling impinging jet
D.W. SNYDER, P.J. SIDES, E.I. KO and S. MAHAJAN, GROWTH KINETICS, CRYSTAL STRUCTURE, AND MORPHOLOGY OF OMVPE-GROWN HOMOEPITAXIAL CdTe, JOURNAL DE PHYSIQUE IV, Colloque C2, suppl. au Journal de Physique 11, Vol. 1, septembre 1991➔ AP CVD modeling impinging jet
Snyder D.W., Metalorganic Chemical Vapor Deposition of Cadmium Telluride, Ph.d. Thesis, Carnegie Mellon University (1990).
Mahajan, R. L., and Wei, C. (1991). Buoyancy, Soret, Dufour, and variable property effects in silicon epitaxy. J. Heat Transfer 113, 688. ➔ MULTI-JET CVD

N.G. GLUMAC and D.G. GOODWIN, Diagnostics and Modeling of Strained Fuel-Rich Acetylene/Oxygen Flames Used for Diamond Deposition, COMBUSTIONAND FLAME, 105: 321-331 (1996)

Harris, S. J., Shin, H. S., and Goodwin, D. G, Diamond films from combustion of methyl acetylene and propadiene, Appl. Phys. Lett. 66:891-893 (1995).

Shin, H. S., and Goodwin, D. G., Appl. Phys. Lett. 66 (21) 2909-2911, (1995)

Murayama, M., Kojima, S., and Uchida, K., J. Appl. Phys. 69:7924-7926 (1991)

Murayama, M., and Uchida, K., Synthesis of Uniform Diamond Films by Flat Flame Combustion of Acetylene/Hydrogen/Oxygen Mixtures, Combust. Flame 91:239-245 (1992);

McCarty, K. F., Meeks, E., Kee, R. J., and Lutz, A. E., Appl. Phys. Lett. 63:1498-1500 (1993).

Glumac, N. G. and Goodwin, D. G., Mater. Lett. Lett. 18 119-122 (1993)

Kim, J. S., and Cappelli, M. A., J. Appl. Phys. 72:5461-5466 (1992)

Kim J.S., Cappelli M.A., Diamond growth under low pressure combustion environments, in Proceedings of the Third International Symposium on Diamond Materials, Diamond Materials edited by John P. Dismukes,K. V. Ravi, The Electrochemical Society, pp. 455

Kim J.S., Combustion synthesis of diamond, PhD Thesis, 1998

Meeks, E., Kee, R. J., Dandy, D. S., and Coltrin, M. E., Combust. Flame 92:144-160 (1993)

Glumac, N. G., and Goodwin, D. G., Thin Solid Films 212:122-126 (1992)

Okkerse M., C.R. Kleijn, H.E.A. van der Akker, M.H.J.M de Croon and G.B. Marin, A two-dimensional simulation model for oxy-acetylene flame CVD diamond films, CVD XV: preceding of the Fifteenth International Symposium on Chemical Vapor Deposition, edited by Mark Donald Allenddorf, M. L. Hitchman, The Electrochemical Society (1993)

M. Okkerse, M. H. J. M. de Croon, C. R. Kleijn, G. B. Marin, H. E. A. van den Akker, Influence of nitrogen on diamond growth in oxyacetylene combustion chemical vapor deposition, JOURNAL OF APPLIED PHYSICS VOLUME 92, NUMBER 7 1 OCTOBER 2002

J.C. Leylegian, H.Y. Sun, C.K. Law, Laminar flame speeds and kinetic modeling of hydrogen/chlorine combustion, Combustion and Flame 143 (2005) 199–210

R. Corbeels, K. Scheller, Proc. Combust. Inst. 10 (1965) 65–75.

C.E. Baukal, B. Gebhart, A review of empirical flame impingement heat transfer correlations, Int. J. Heat and Fluid Flow 17: 386-396, 1996

E.G. Jackson, J.K. Kilham, Heat transfer from combustion products by forced convection, Ind. Engng. Chem. 48(11) (1956) 2077-2079

J.M. Béer, N.A. Chigier, Impinging jet flames, Combust. Flame 12 (1968) 575-586.

A. Milson, N.A. Chigier, Studies of methane-air flames impinging on a cold plate, Combust. Flame 21 (1973) 295-305

J.K. Kilham, M.R.I. Purvis, Heat transfer from hydrocarbon-oxygen flames, Proc. of the Eleventh Int. Symp. on Combust. The Combustion Institute, Pittsburg, PA (1967)

J. A. Miller, M. C. Branch, W. J. McLean, D. W. Chandler, M. D. Smooke, and R. J. Kee, in Proceedings of the Twentieth Symposium (International) on Combustion, The Combustion Institute, Pittsburgh, Pennsylvania, 1985, p. 673

Y. Reuven, M. D. Smooke, and H. Rabitz, Sensitivity Analysis of Boundary Value Problems: Application to Nonlinear Reaction-Diffusion Systems, Yale University Mechanical Engineering Department Report ME-104-85, 1985, pp.80-96